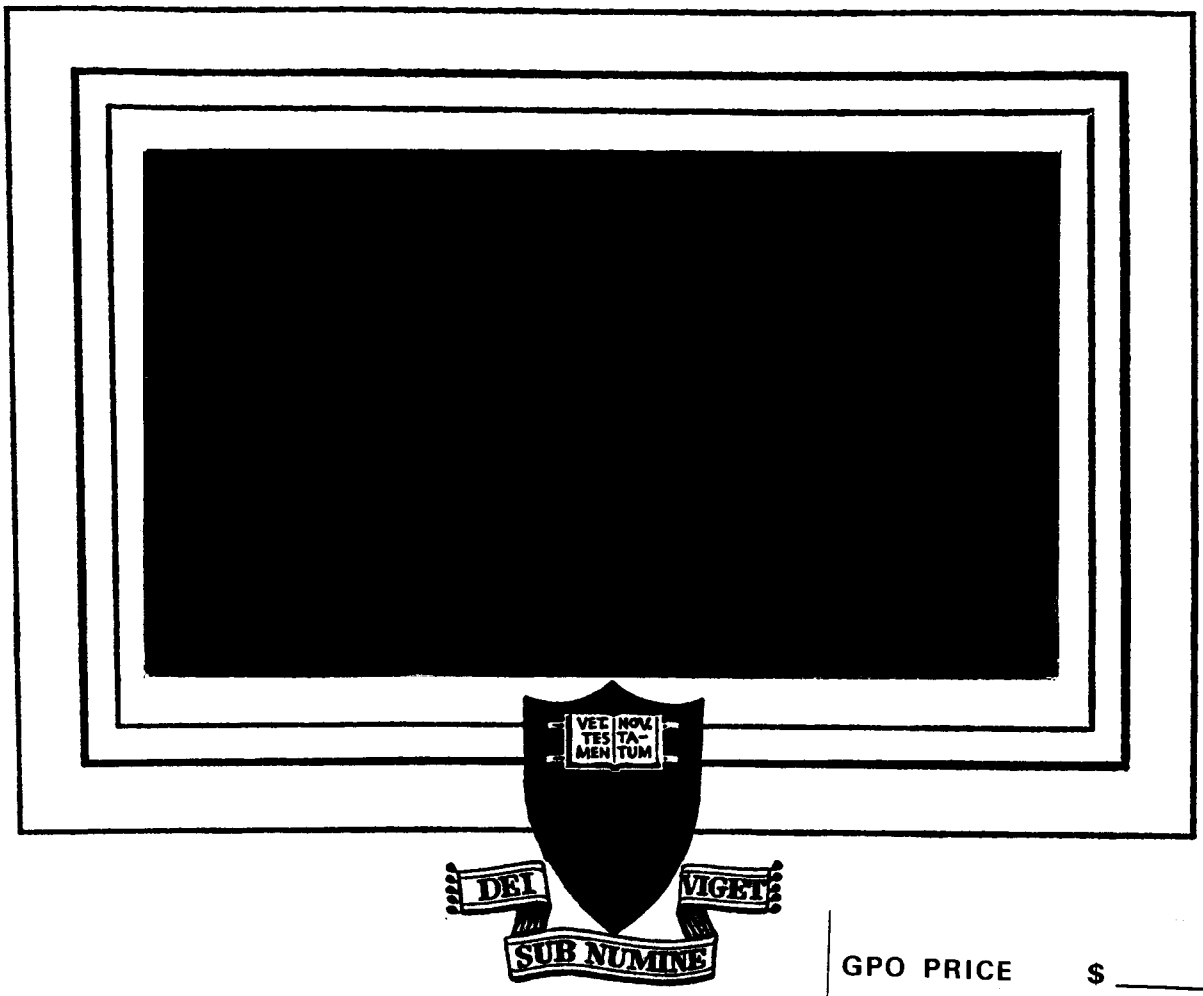

PRINCETON UNIVERSITY

DEPARTMENT OF AERONAUTICAL ENGINEERING

NATIONAL AERONAUTICS AND SPACE ADMINISTRATION

GRANT NO. NsG-389

A Technical Report on

under

CONCEPTUAL DESIGN STUDY OF A LIQUID-CORE NUCLEAR ROCKET

Aeronautical Engineering Laboratory

Report No. 665

Prepared by: Seymour T. Nelson (Aug 64)

Seymour T. Nelson
Assistant in Research

Approved by: Jerry Grey

Jerry Grey
Associate Professor

September 1963

Guggenheim Laboratories for the Aerospace Propulsion Sciences
PRINCETON UNIVERSITY
Princeton, New Jersey

TABLE OF CONTENTS

LIST OF ILLUSTRATIONS AND TABLES

LIST OF SYMBOLS

A = area, (cm^2) Eq. (140)

B^2 = buckling, (cm^{-2}) Eq. (26)

C = total number of channels per fuel element Eq. (139)

D = diffusion coefficient, (cm) Eq. (15)

D = diameter, (cm) Eq. (35)

F = thrust (equivalent mass units, viz., gm, metric tons and lb. are used) Eq. (102)

H = height (length), (cm) Eq. (30)

I_{sp} = specific impulse, (sec) Eq. (99)

J = variable defined by Eq. (277)

K = variable defined by Eq. (279)

L = thermal diffusion length, (cm) Eq. (13)

M = migration length, (cm) Eqs. (18) and (20)

M = mass, (gm or metric tons) Eq. (42)

$\dot{M}$ = mass flow rate, (gm/sec) Eq. (103)

N = particle density, (cm^{-3}) Eq. (9)

N = number of fuel elements in the core Eq. (71)

N = variable defined by Eq. (278)

P = maximum number of fuel elements along a diameter of the core Eq. (71)

Q = rate of heat transfer, (cal/sec), Eq. (271)

R = radius, (cm) Eq. (29)

R^*, R_o^* = defined by Eqs. (137) and (136), respectively (cm)

Re = Reynolds number based on bubble diameter, Eq. (279)

T = thickness of beryllium reflector, (cm) Eq. (37)

T = temperature, (^{o}K) Eq. (97)

V = volume, (cm^3 or m^3) Eq. (31)

V = $T_{surface} - T_{center}^{initial}$ (^{o}K), Eq. (216)

Y = average number of bubbles in the core at any instant Eq. (191)

a = area, (cm^2) Eq. (128)

a = bubble radius, (cm) Eq. (211)

b = thickness of a spherical cap bubble, (cm) Eq. (123)

c_p = specific heat at constant pressure, (cal/gm-^{o}K) Eq. (263)

d = dilution ratio Eqs. (9)-(10)

d = diameter, (cm) Eq. (75)

f = thermal utilization factor Eq. (9)

f = ratio of bubble diameter to orifice diameter at breakoff Eq. (200)

$f(\theta)$ = integrand of J Eq. (277)

g = centrifugal or gravitational acceleration (cm/sec^2) Eq. (122)

j = summation index Eq. (71)

k = thermal conductivity, (cal/sec-cm-^{o}K) Eq. (259)

k_∞ = infinite multiplication factor Eq. (12)

m = mass, (gm) Eq. (48)

n = index of summation Eq. (217)

$\dot{n}$ = molar flow rate (moles/sec) Eq. (298)

p = resonance escape probability Eq. (1)

p = pressure, (dyne/cm^2, atm or psi) Eq. (98)

p_v = vapor pressure, (atm) Eq. (290)

q = heat transfer rate per unit area (cal/sec-cm^2) Eq. (274)

r = radius, (cm) Eq. (122)

s = center-to-center separation distance, (cm) Eq. (132)

t = fuel element wall thickness, (cm) Eq. (79)

u = velocity, (cm/sec) Eq. (122)

v = volume, (cm^3) Eq. (126)

x = mole fraction Eq. (293)

y = average number of bubbles per fuel element at any instant Eq. (190)

Γ = average number of bubbles in a channel at any instant Eq. (188)

Π = wall porosity Eq. (201)

Σ_a = macroscopic absorption cross section (cm^{-1}) Eq. (9)

α = thermal diffusivity (cm^2/sec) Eq. (213)

δ = reflector savings, (cm) Eq. (38)

ε = fast fission factor Eq. (2)

ε = I_{sp} error, (sec) Eq. (316)

η = average number of fast fission neutrons emitted for each thermal neutron absorbed in the fissionable material Eq. (11)

θ = angle (deg or radius) Eq. (123)

λ_{tr} = transport mean free path (cm) Eq. (15)

μ = coefficient of viscosity, (poise) Eq. (281)

$\bar{\mu}_o$ = average cosine of the scattering angle per collision in the laboratory system Eq. (15)

ν = rotational frequency, (rev/sec) Eq. (145)

ξ = variable of integration Eq. (218)

ρ = density, (gm/cm^3) Eq. (41)

ρ' = effective density of liquid fuel, taking account of bubble population (gm/cm^3) Eqs. (169)-(170)

σ = microscopic cross section, (cm^2 or barn = $10^{-24} cm^2$) Eq. (3)

σ = stress, ($dyne/cm^2$ or psi) Eq. (152)

τ = Fermi age, (cm^2) Eqs. (17) and (19)

τ = time, (sec) Eq. (204)

Φ = bubble frequency (per channel), (cm^{-1}) Eq. (138)

ω = angular velocity, (rad/sec) Eq. (145)

$\mathfrak{M}$ = molecular mass, (a.m.u.) Eq. (100)

$\mathfrak{N}$ = dimensionless acceleration Eq. (150)

$\mathfrak{R}$ = universal gas constant

= 8.314×10^7, ($erg/^oK/g\text{-}mole$) Eq. (141)

$\mathfrak{V}$ = void fraction (hydrogen is considered as "void") Eq. (14)

$\mathfrak{L}$ = radial distance measured inward from station "o", (cm) Eq. (206)

$\mathfrak{v}$ = $T_{interior} - T_{center}^{initial}$, ($^oK$) Eq. (214)

$\mathfrak{v}_c$ = $T_{center} - T_{center}^{initial}$, ($^oK$), Eq. (215)

SUPERSCRIPT

lat ⟶ lateral Eq. (132)

rad ⟶ radial

o ⟶ refers to pure substance

t ⟶ denotes "thermal" value, i.e., at 293°K (0.0253 ev) Eq. (4)

* ⟶ "effective" value, taking into account the void fraction Eq. (14)

SUBSCRIPT

A,B,C ⟶ thrust levels A,B,C (defined by Eqs. (102), (104), (106), respectively)

C ⟶ carbon Eq. (7)

U ⟶ uranium 235 Eq. (3)

UC_2 ⟶ uranium (di-) carbide Eq. (48)

Zr ⟶ zirconium Eq. (5)

ZrC ⟶ zirconium carbide Eq. (48)

a ⟶ absorption Eq. (3)

b ⟶ bubbles Eq. (111)

c ⟶ bare (critical) core Eq. (26)

c ⟶ chamber Eq. (97)

e ⟶ equivalent Eq. (131)

f ⟶ fuel Eq. (46)

h ⟶ hydrogen Eq. (90)

h ⟶ hydrostatic Eq. (168)

i ⟶ specie i Eq. (14)

i ⟶ inner Eq. (79)

i ⟶ intersticial Eq. (88)

m ⟶ moderator (C) Eq. (13)

m ⟶ mean Eq. (153)

o ⟶ outer Eq. (79)

r ⟶ reflector Eq. (41)

s ⟶ scattering Eq. (15)

t ⟶ total Eq. (56)

w ⟶ wall Eq. (89)

1,2,3 ⟶ matrix geometries 1,2,3 (specified by Eqs. (72), (73), (74), respectively)

01,12,23,24 ⟶ defined in paragraph following Eq. (205)

MISCELLANEOUS

$\langle x \rangle$ = mean value of x averaged over a Maxwell-Boltzmann energy (temperature) distribution Eq.(3)

erfc x = complementary error function of x (defined by Eq. (218))

Δx = increment of x Eq. (270)

x' = corrected value of x Eq. (308)

I. SUMMARY

A conceptual design study for a liquid-core nuclear rocket was performed, based on realistic (in fact, conservative) assumptions regarding nucleonics, bubble flow and heat transfer and fuel-mixture vapor loss. The postulated reactor configuration was a matrix of mechanically-driven rotating hollow cylinders composed of a fissionable fuel mixture (UC_2 heavily diluted with ZrC) and cooled by a radially-inward flow of hydrogen, operating with the inner surface of the cylinder in the molten state.

Parameter optimization calculations demonstrated that the vacuum specific impulse of the system was limited by loss of fuel-mixture vapor to slightly greater then 1200 seconds at engine thrust/weight ratios over the range 0.05 to 0.5, with chamber pressures in the range 3 to 100 atm, peak molten-surface temperatures of 3600 to 3800°K, and ZrC/UC_2 dilution ratios between 250 and 1500. Thrust levels were limited by bubble flow area (i.e., fuel-element surface area) rather than heat transfer. Fuel element diameters may be of the order of an inch and speeds of rotation of the order of 5,000 rpm. Engineering design, control, dynamic response, and operational characteristics are not discussed in this conceptual study.

It was concluded that the performance of the liquid-core nuclear rocket (in terms of specific impulse and thrust/weight ratio) was sufficiently interesting to warrant both more careful system analyses and systematic research programs

in the critical areas of bubble flow and heat transfer in liquid ceramic or cermet media under high-gravity conditions, fuel-element component vapor pressures, and basic operational problems such as coolant-passage "freezing-in" on shutdown.

II. INTRODUCTION

A. Performance

The liquid core nuclear rocket represents the next step beyond solid core systems of the type now under development in the Rover program. It holds promise of performance at least 50% greater than that of solid core reactors at thrust-to-weight ratios of 0.1 or more.

The principal attraction of the liquid core reactor lies in the fact that it permits operation at temperatures of 3600 - 3800°K. At these temperatures and moderate chamber pressures (10 - 30 atm), dissociation of the hydrogen propellant is significant, resulting in a vacuum specific impulse exceeding 1200 seconds.

B. Core Geometry

The core geometry is shown in Figure 1. Although throughout the present analysis we will assume a multiplicity of vortex-tube fuel elements (in the form of a hexagonal array), the alternative scheme, consisting of a single large vortex, is not precluded as a possibility. The matrix geometry was selected for detailed investigation for two reasons:

1. It provides for a much more homogeneous distribution of fuel throughout the core volume, and consequently far better nucleonic properties. A single-vortex core would necessitate a fuel annulus which is thin compared with the core diameter; such a "shell" geometry resembles a thin slab core and is very unfavorable from the standpoint of neutron economy.
2. For a fixed specific impulse (performance being limited by materials properties, as usual), the thrust is proportional to the total fuel element surface area. The latter increases with the number of fuel elements in the core.

C. Restart Problem

The restart problem, while quantitatively neglected in the present study, will of course affect and be affected by the optimum core geometry. The most attractive proposal for solving this problem in a single-vortex core is due to L. Crocco, (1)* who suggested that the porous chamber wall be fabricated from the identical fuel material as the adjacent liquid annulus (e.g., a mixture of ZrC and UC_2). Initially the fuel is all solid. At startup, the inner surface of the

---

* Numbers in parentheses indicate references listed on page 71.

fuel annulus melts first. The solid/liquid interface recedes until full power is achieved, at which time the interface has reached its steady-state position. Shutdown is then simply a reversal of this process. The only problem is to ensure that a sufficient number of uniformly distributed channels are frozen into the fuel so that the latter retains a porosity appropriate for restarting. This problem is certainly not trivial, and represents a critical area for subsequent experimental evaluation. It does, however, supplant several alternative problems (arising from inhomogeneity of fuel element composition) which are probably even more formidable.

III. NUCLEONICS

A. Assumptions

The reactor is calculated on the basis of age-diffusion theory, whose results should be of sufficient accuracy to fix the core properties to within an order of magnitude. On the basis of the representative reactor thus determined, we examine in Section IV the feasibility of the liquid core nuclear rocket concept from the standpoint of overall performance potential. Reactor kinetics, and indeed all other transient phenomena associated with the system, are beyond the scope of this study.

Consistent with the approximation inherent in the use of age-diffusion theory, we simply replace hydrogen propellant by void (since the moderating effect of the hydrogen tends to just about offset its neutron absorption cross section). Moreover, we assume that both the fuel and the void are uniformly distributed throughout the core. The void fraction is denoted by $\mathcal{V}$. The fissionable material is taken to be U-235 in the form of UC_2. The latter was chosen over UC for two reasons:

1. Vapor pressure data on UC_2 are available in the unclassified literature, but not on UC.
2. UC has higher melting and boiling points than UC_2 and therefore may well ultimately be selected over UC_2; in the meantime, choice of the latter represents a degree of built-in conservatism which is always desirable in feasibility studies.

At one atmosphere pressure, UC_2 boils at about 4370°K. The peak fuel temperature is taken as 4300°K* and

---

* This value was selected before any results were available on the vapor entrainment loss problem (see Part IV, Section J). Subsequent analysis has shown that the optimum temperature is about 3600°K for operation at 10 atm chamber pressure and 3800°K for 30 atm. A revised nucleonic analysis based on these lower temperatures (and, incidentally, including U-233 as an alternate fissionable material) is now in progress. Since all the calculations are based on neutron cross sections which are averaged over a Maxwell-Boltzmann distribution about the chamber temperature, it is clear that the newer temperature values will result in reactors of smaller critical size and mass than for T = 4300°K. An even greater improvement will be manifest in the U-233 reactors. The (interim) results presented here should therefore be regarded as somewhat pessimistic.

it is assumed that the hydrogen propellant achieves substantially this temperature before expansion through the nozzle. (In Part IV it will be shown that this assumption is correct). The following two factors tend to make this choice of chamber temperature more acceptable than would otherwise be the case:

1. The chamber pressure is taken greater than 1 atmosphere for all calculations, with a tentative design point at 10 atmospheres (see Part IV).
2. The UC_2 is "diluted" by ZrC in the ratio of d molecules of ZrC to each molecule of UC_2. The diluent was chosen on the basis of a combination of good nucleonic properties (particularly a low neutron absorption cross section) and good high temperature characteristics. At one atmosphere, ZrC boils at about 5370°K. At 4300°K its vapor pressure is much less than that of UC_2; its principal function is to reduce the vapor entrainment loss of fissionable material. Some relevant materials properties are summarized in Table 1.

The reactor is assumed to be a thermal reactor, the neutrons being thermalized to 0.37 ev, which corresponds to 4300°K. All cross sections are averaged over a Maxwell-Boltzmann distribution about this temperature. (Were we to assume thermalization to 293°K, the results would of course be too optimistic).

It is assumed that the moderating effect of Zr is negligible, the only important moderator being C. This is a fairly good approximation, whose effect will be to make the critical size estimate slightly conservative.

Also consistent with the present approximation are the compensating assumptions that resonance absorption and fast fission are both negligible. Thus we take

$$p \equiv \text{resonance escape probability} \approx 1, \qquad (1)$$

$$\epsilon \equiv \text{fast fission factor} \approx 1. \qquad (2)$$

B. Age-Diffusion Analysis

Based on data in ANL - 5800, or from Bussard and De Lauer (2), p. 160, Figure 5-8, we have

$\langle \sigma_a \rangle_U \equiv$ microscopic absorption cross section of U-235, averaged over a Maxwell-Boltzmann distribution about 4300°K (corresponding to 0.37 ev)

$$= 120 \text{ barns.} \qquad (3)$$

Now,

$(\sigma_a^t)_{Zr} \equiv$ microscopic absorption cross section of Zr at 293 °K

$$= 0.185 \text{ barns}. \qquad (4)$$

Assuming 1/v-absorption by Zr, then

$$\langle \sigma_a \rangle_{Zr} = \frac{(\sigma_a^t)_{Zr}}{1.128} \left(\frac{293}{4300} \right)^{1/2}. \qquad (5)$$

(See, e.g., Glasstone and Sesonske (3)- p. 77). Substituting

Eq. (4) into Eq. (5) gives

$$\langle \sigma_a \rangle_{Zr} = 4.28 \times 10^{-2} \text{ barns.} \tag{6}$$

Similarly,

$$(\sigma_a^t)_C = 3.73 \times 10^{-3} \text{ barns,} \tag{7}$$

so that

$$\langle \sigma_a \rangle_C = 8.62 \times 10^{-4} \text{ barns.} \tag{8}$$

The thermal utilization factor is

$$f = \frac{\langle \Sigma_a \rangle_U}{\langle \Sigma_a \rangle_U + \langle \Sigma_a \rangle_{Zr} + \langle \Sigma_a \rangle_C}$$

$$= \frac{\langle \sigma_a \rangle_U}{N_{UC_2}\langle \sigma_a \rangle_U + N_{ZrC}\langle \sigma_a \rangle_{Zr} + (2N_{UC_2} + N_{ZrC})\langle \sigma_a \rangle_C}$$

$$= \frac{\langle \sigma_a \rangle_U}{\langle \sigma_a \rangle_U + d\langle \sigma_a \rangle_{Zr} + (2+d)\langle \sigma_a \rangle_C} ,$$

where the Σ_a's are the macroscopic absorption cross sections, the N's are the particle densities (molecules/cm^3), and

$$d \equiv \text{dilution ration} = N_{ZrC}/N_{UC_2}. \tag{10}$$

Since $p\epsilon \approx 1$ by Eqs. (1) and (2), and

$$\eta_{U\text{-}235} = 2.06, \tag{11}$$

the infinite multiplication factor is

$$k_\infty = \eta f p \epsilon \approx \eta f = 2.06\, f \tag{12}$$

Since the reactor is thermal and C is taken to be the only important moderator, we may write

$$L^2 = L_m^2 \ (1 - f), \tag{13}$$

where L and L_m are the thermal diffusion lengths in the core and for pure graphite, respectively.

We must now take into account the void fraction, ν. Thus, the effective particle density for specie i, N_i^* is

$$N_i^* = (1 - \nu) \ N_i. \tag{14}$$

Since

$$L_m^2 = \left(\frac{D^t}{\Sigma_a^t}\right)_m = \left(\frac{\lambda_{tr}}{3\Sigma_a^t}\right)_m$$

$$= \left[\frac{1}{3\Sigma_a^t \Sigma_s^t (1-\bar{\mu}_o)}\right]_m$$

$$= \left[\frac{1}{3\sigma_a^t \sigma_s^t (1-\bar{\mu}_o) N^2}\right]_m , \tag{15}$$

it follows from Eq. (14) that

$$L_m^{*2} = \frac{L_m^2}{(1-\nu)^2} , \tag{16}$$

where L_m^* is the effective thermal diffusion length in the moderator.

Analogously,

$$\tau_m^* = \frac{\tau_m}{(1-\nu)^2} \tag{17}$$

and

$$M^{*2} = \frac{M^2}{(1-\nu)^2} , \tag{18}$$

where

$$\tau \equiv \text{Fermi age} \equiv (\text{slowing down length})^2, \tag{19}$$

$$M \equiv \text{migration length} \equiv (L^2 + \tau)^{1/2}. \tag{20}$$

From Reference (3), p. 147, Table 3.5, we find:

$$L_m = 64.2 \text{ cm}, \tag{21}$$

$$\sqrt{\tau_m} = 18.7 \text{ cm}. \tag{22}$$

Thus

$$\tau^* = \tau_m^* = \frac{350}{(1-\nu)^2} , \tag{23}$$

$$L^{*2} = \frac{L_m^2 (1-f)}{(1-\nu)^2} = \frac{4122\,(1-f)}{(1-\nu)^2} , \tag{24}$$

$$M^{*2} = \tau^* + L^{*2} = \frac{4122(1-f)+350}{(1-\nu)^2} . \tag{25}$$

A preliminary estimate for the buckling, B_c^2, is

$$\left(B_c^2\right)_{\text{prelim.}} = \frac{k_\infty - 1}{M^{*2}} \,. \tag{26}$$

In order to cross-plot some of the final results, 30 different reactors have been calculated, representing all combinations of d = 5, 10, 50, 100, 500 and 1000 with ν = 10%, 20%, 30%, 40%, and 50%. Table 2 presents the results of the preliminary calculations.

The next step is to solve the age-diffusion equation,

$$e^{-B_c^2 \tau^*} = \frac{1 + L^{*2} B_c^2}{k_\infty} \,, \tag{27}$$

for the buckling. This has been done by the usual trial-and error iterative method. The results, along with all the subsequent results (see below) appear in Table 3.

The radius of a bare core is given by

$$B_c^2 = \left(\frac{2.405}{R_c}\right)^2 + \left(\frac{\pi}{H_c}\right)^2 \,, \tag{28}$$

where

$$R_c \equiv \text{radius of bare core,} \tag{29}$$

$$H_c \equiv \text{height (length) of bare core.} \tag{30}$$

Letting

$$V_c \equiv \text{volume of bare core,} \tag{31}$$

then

$$V_c = V_{c_{min}} = \frac{148}{B^3_{c_{min}}} \tag{32}$$

for

$$H_c = 1.847\ R_c \equiv H_{c_{min}}\ , \tag{33}$$

where the subscript min refers to minimized <u>volume</u>. Thus, substituting Eq. (33) into Eq. (28) gives

$$B^2_{c_{min}} = 8.674/R^2_c\ . \tag{34}$$

Instead of choosing H_c in this fashion, i.e., so as to minimize the critical mass, let us lengthen the core a bit. (Under no circumstances is it worthwhile to consider <u>large</u> departures from minimum volume geometry). This will have the effect of reducing R_c slightly and also make the critical mass estimate tend to be a little conservative. We therefore adopt the following configuration as "standard"

throughout the analysis:

$$H/D = 1.5. \tag{35}$$

Substituting $H_c = 3R_c$ into Eq. (28) and rearranging yields

$$R_c^2 = 6.88/B_c^2. \tag{36}$$

C. Reflector Savings

Let us also adopt a "standard reflector", consisting of a one thermal diffusion length thickness (21 cm) of Be, in the form of a cylindrical annulus plus two flat end plates whose diameter is the same as the outer diameter of the annulus. Of course the actual distribution of reflector material will resemble that shown in Figure 1; for simplicity we assume that the total volume of the forward reflector cap and the aft (nozzle) reflector equals that of the two end plates.

We have selected Be as the reflector material and a single thermal diffusion length as the thickness on the basis of general nuclear rocket considerations. Experience indicates that Be and BeO are the optimum materials for flight applications; the latter is excluded because of reflector contact with hydrogen. Also, a single diffusion length is a good compromise between reflectivity and weight.

According to Reference (3), p. 174, Figure 4.5, for

$$T \doteq \text{Be thickness} = 21 \text{ cm}, \tag{37}$$

the reflector savings is

$$\delta = 16 \text{ cm}. \tag{38}$$

The reflector volume is

$$V_r = 2\, V_{\text{end plate}} + V_{\text{annulus}}$$

$$= 2\,\pi(R + T)^2 T + \pi[(R+T)^2 - R^2]\, 3R, \tag{39}$$

where

$R \equiv$ radius of reflected core (but excluding the reflector)

$$= R_c - \delta. \tag{40}$$

The density of Be is

$$\rho_r = 1.84 \text{ gm/cm}^3. \tag{41}$$

The total reflector mass is obtained by combining Eqs. (37)-(41):

$$M_r = 5.78\,(168\, R_c^2 - 2289\, R_c + 12{,}138), \tag{42}$$

where R_c is in cm and M_r in grams.

The overall core diameter (including the reflector) is

$$D_t = 2\,(R + T). \tag{43}$$

The length of the core (excluding the reflector) is

$$H = 3R. \tag{44}$$

The core volume (excluding the reflector), i.e., void plus fuel volume, is

$$V = 3\,\pi\, R^3. \tag{45}$$

The fuel volume is therefore

$$V_f = (1 - \mathcal{V}) \, 3\pi R^3. \tag{46}$$

The fuel mass is then

$$M_f = \rho_f V_f , \tag{47}$$

where

$$\rho_f = N_{ZrC} m_{ZrC} + N_{UC_2} m_{UC_2}$$

$$= N_{ZrC} \left(m_{ZrC} + \frac{m_{UC_2}}{d} \right) , \tag{48}$$

where m_{ZrC} and m_{UC_2} are the masses (in grams) of the ZrC and UC_2 molecules, respectively:

$$m_{ZrC} = 1.715 \times 10^{-22} \text{ grams}, \tag{49}$$

$$m_{UC_2} = 4.30 \times 10^{-22} \text{ grams} . \tag{50}$$

Moreover, from Reference (2), p. 155, Table 5-5,

$$N_{ZrC} = 3.96 \times 10^{22} \text{ molecules/cm}^3. \tag{51}$$

Thus

$$M_f = (3.96) \left[1.715 + \frac{4.30}{d} \right] V_f . \tag{52}$$

Of this, there are

$$M_{UC_2} = (3.96)(4.30) \, V_f/d = 17.0 \, V_f/d \tag{53}$$

grams of UC_2, of which

$$M_U = (235/259)\, M_{UC_2} = 0.9075\, M_{UC_2} \qquad (54)$$

grams are U-235. Assuming that the latter costs approximately \$10/gram, the fuel inventory cost is

$$(\text{U-235 cost}) = \$10\, M_U . \qquad (55)$$

Neglecting the control system (and a host of other components as well as the hydrogen in the core), the total reactor mass is

$$M_t = M_f + M_r . \qquad (56)$$

Figures 2 - 8 present the results of the foregoing calculations in graphical form. From inspection of these figures, the following reactor has been selected as representative of the type which appears most favorable for rocket applications:

$$\sqrt{} = 50\%, \qquad (57)$$

$$d = 500, \qquad (58)$$

$$R_c = 163.9 \text{ cm}, \qquad (59)$$

$$R = 147.9 \text{ cm}, \qquad (60)$$

$$D_t = 337.8 \text{ cm } (= 11.08 \text{ ft}), \qquad (61)$$

$$H = 443.7 \text{ cm}, \qquad (62)$$

$$V = 30.45 \text{ m}^3, \qquad (63)$$

$$V_f = 15.225 \text{ m}^3, \qquad (64)$$

$$_f = 6.83 \text{ gm/cm}^3, \qquad (65)$$

$$M_f = 104.0 \text{ m.t. (metric tons)}, \qquad (66)$$

$$M_{UC_2} = 0.518 \text{ m.t.}, \qquad (67)$$

$$M_U = 0.471 \text{ m.t.}, \qquad (68)$$

$$M_r = 24.0 \text{ m.t.}, \qquad (69)$$

$$M_t = 128.0 \text{ m.t.} \tag{70}$$

This reactor is indicated by a small circle in each of Figures 2 - 8; it will form the basis for the calculations of Part IV.

D. Fuel Element Configuration

One important reactor property still unspecified is N, the number of vortex tubes (fuel elements). As will be recalled, we assume a hexagonal array of tubes. Let P be the maximum number of tubes which can be placed along a diameter of the core. Then it may easily be verified that

$$N = N(P) = 1 + \sum_{j=1}^{P} 3\,(j - 1) \tag{71}$$

In selecting a particular configuration (which according to Eq. (71) is completely specified by the set (N, P), the following considerations should be borne in mind:

1. Reasons for decreasing the vortex tube diameter (i.e., increasing N):

   A. The total fuel element surface area is increased. Hence the propellant flow rate and therefore the thrust are also increased.

   B. Homogeneity of the core is improved, and therefore the reactor more closely approaches the ideal case assumed in the nucleonic calculations. (Once N exceeds about 100,

this reason greatly diminishes in importance).

2. Reasons for increasing the vortex tube diameter (i.e., decreasing N):

A. Problems of tube fabrication are ameliorated.

B. For a fixed centrifugal acceleration, the requisite angular velocity is decreased.

C. For the range of configurations of practical interest, the thickness of the liquid fuel annulus is increased. (It varies essentially as $N^{-1/2}$). This means that the heat transfer problem is somewhat eased, since each bubble has a longer path length within the fuel. It is later shown however, that adequate heat transfer is achieved within a very small liquid depth.

On the basis of these considerations, let us select the following three configurations for further study:

$$\text{Matrix 1:} \quad (N_1, P_1) = (127,13), \tag{72}$$

$$\text{Matrix 2:} \quad (N_2, P_2) = (1017,37), \tag{73}$$

$$\text{Matric 3:} \quad (N_3, P_3) = (9919, 115). \tag{74}$$

The fuel element diameter is

$$d = \frac{2R}{P} . \tag{75}$$

Thus, in particular, we have

$$(d)_1 = 22.754 \text{ cm} = 8.95", \tag{76}$$

$$(d)_2 = 7.995 \text{ cm} = 3.15", \tag{77}$$

$$(d)_3 = 2.572 \text{ cm} = 1.01". \tag{78}$$

E. Fuel Element Wall Thickness

The fuel element walls, it will be recalled, are assumed to consist of unloaded ZrC. Heretofore we have tacitly assumed their thickness to be negligible. That is, we have ignored the effects upon overall core diameter and dilution ratio of this volume of pure ZrC. The reason this was done is as follows: The thickness, t, (and hence the inner diameter, d_i) of the solid wall is determined from hoop and thermal stress considerations. The hoop stress depends on the angular velocity of the liquid fuel in the tube (which is as yet undetermined) and the thermal stress depends on certain materials properties for which data are presently unavailable in the unclassified literature. It is therefore necessary to defer actual calculation of d_i. In the meantime, subject to later re-examination, let us arbitrarily choose the wall thickness to be

$$t \equiv \frac{d_o - d_i}{2} = \frac{d_i}{15} . \qquad (79)$$

It is in order to allow most conveniently for replacement of Eq. (79) by a subsequently calculated value that we have excluded the effects of non-zero t upon the nucleonic calculations leading up to the "standard" core specified by Eqs. (57)-(70). For the present, we merely enlarge the critical dimensions and total mass so as to just accomodate the fuel element walls, in accordance with the convention adopted in Eq. (79). Of course the actual

increases will be affected by nucleonic considerations, the net result being that addition of the wall mass, M_w, will increase the bare core mass by an amount less than M_w, and similarly for the size increase. This is because the moderating effect of the added ZrC partially offsets its size and mass. We will simply ignore this refinement and recognize the intrinsic conservatism of the approximation.

Thus, since the values of d given by Eqs. (75)-(78) really represent d_i, we have:

$$d_o = \frac{17}{15} d_i, \tag{80}$$

so

$$(d_o)_1 = 25.783 \text{ cm} = 10.14", \tag{81}$$

$$(d_o)_2 = 9.061 \text{ cm} = 3.565", \tag{82}$$

$$(d_o)_3 = 2.915 \text{ cm} = 1.147", \tag{83}$$

The enlarged core radius is therefore

$$R = \frac{P\, d_o}{2} = 167.6 \text{ cm}. \tag{84}$$

Hence

$$D_t = 2R + 42 = 377.2 \text{ cm} = 12.38 \text{ ft} \tag{85}$$

and

$$H = 3R = 502.8 \text{ cm}. \tag{86}$$

The total core volume (excluding reflector) is then

$$V = 3\pi R^3 = 44.4 \text{ m}^3. \tag{87}$$

Of this, the interstices between the individual fuel elements and between the inner surface of the reflector and the fuel elements account for

$$V_i = 11.16 \text{ m}^3, \tag{88}$$

where we have taken the average for the three matrices. (The individual values differ from each other by very little). V_i may also be thought of as the pre-injection propellant manifold volume.

The aggregate fuel element wall volume has an average value for the three matrices of

$$V_w = 7.32 \text{ m}^3. \tag{89}$$

This leaves a total of 25.92 m^3, divided equally (we assume) between fuel and hydrogen ("void"):

$$V_f = V_h = 12.96 \text{ m}^3. \tag{90}$$

The fact that this is 14.9% less than the value for the original standard reactor (of Eq. (64)) will simply be disregarded. That we may do this without introducing greater errors than are compatible with the degree of accuracy of previous assumptions and calculations should be evident from earlier remarks. (The discrepency arises, incidentally, from the fact that we originally assumed V_f to be simply V/2). Note that we still assume that V_h, the hydrogen volume <u>within</u> the fuel elements (i.e., excluding V_i) equals V_f. This means that the void fraction for the interior of a single fuel element is still taken to be 50%, but the actual overall core void fraction is now really 54.3%.

The reflector volume is, from Eq. (39),

$$V_r = 16.53 \text{ m}^3, \tag{91}$$

Thus

$$M_r = 30.40 \text{ m.t.}, \tag{92}$$

a value which is nearly 27% greater than that given by Eq. (69).

The fuel mass is

$$M_f = 88.50 \text{ m.t.}, \tag{93}$$

of which

$$M_{UC_2} = 0.44 \text{ m.t.} \tag{94}$$

are UC_2, of which, in turn,

$$M_U = 0.40 \text{ m.t.} \tag{95}$$

are U-235. Thus we see that, at \$10/gm, and assuming that in-flight replenishment is negligible, the net fissionable material cost is less than \$4 million.

The total mass of the fuel element walls is

$$M_w = 49.78 \text{ m.t.} \tag{96}$$

Neglecting (as before) the mass of the hydrogen in the core and the mass of the nozzle, we find that the total reactor mass is

$$M_t = M_f + M_w + M_r = 168.7 \text{ m.t.} \tag{97}$$

IV. SYSTEM ANALYSIS

A. Chamber Pressure and Propellant Mass Flow Rate

The maximum temperature, T_c, of propellant gas

in the chamber is fixed by materials limitations. In Section III this temperature was taken to be

$$T_c = 4300^{\circ}K^{*}$$

This value will be presupposed in all subsequent calculations.

In order to maximize the thrust, F, we must, among other things, maximize the density, ρ_c. According to the perfect gas law, ρ_c is proportional to the chamber pressure, p_c, since T_c is specified. Thus we see that it is desirable to maximize p_c.

On the other hand, the specific impulse, I_{sp}, varies as $\mathfrak{m}^{-1/2}$, $\mathfrak{m}$ being the mean molecular mass of the exhaust gas. As p_c is increased, the fractional dissociation decreases, so $\mathfrak{m}$ increases, thereby lowering performance (I_{sp}). In other words, from a performance standpoint, it is desirable to minimize p_c.

The following choice of p_c represents a compromise based upon trial calculations, between these conflicting requirements:

$$p_c = 10 \text{ atm} = 146.960 \text{ psi}$$
$$= 1.0132 \times 10^7 \text{ dynes/cm}^2 \qquad (98)$$

This value is adopted for the sample case, and full pressure dependence is illustrated later in the report.

---

* See footnote on page 5.

Table I of a technical note by C. R. King (4) gives the vacuum specific impulse for an equilibrium composition of pure hydrogen with p_c = 10 atm and pressure ratio = 3000 as:

$$I_{sp} = 1594.3 \text{ sec for } T_c = 4200^{\circ}K \text{ and}$$
$$I_{sp} = 1687.9 \text{ sec for } T_c = 4400^{\circ}K.$$

These cases correspond to nozzle area ratios of 221.21 and 229.33, respectively -- values which may certainly be achieved without excessive nozzle weight, since the propellant is hydrogen. The arithmetic mean of these specific impulse values is 1641.1 sec. Let us therefore assume that for the case under consideration, neglecting, for the moment, any fuel-element vapor contamination,

$$I_{sp_v} = 1600 \text{ sec.} \tag{99}$$

At the specified chamber temperature and pressure we have, according to Figure 11 of King's paper,

$$\mathfrak{M}_c = 1.465 \text{ a.m.u.} \tag{100}$$

Of course for the cool gas (at injection),

$$\mathfrak{M}_o = 2.016 \text{ a.m.u.} \tag{101}$$

We will examine the implications of the following representative thrust levels:

Case A:,

$$F_a = 10^7 \text{ gm} = 10 \text{ metric tons} - 22{,}050 \text{ lb}, \tag{102}$$
$$\dot{M}_A = F_A/I_{sp} = 6.25 \times 10^3 \text{ gm/sec.} \tag{103}$$

Case B:

$$F_B = 5 \times 10^7 \text{ gm} \approx 50 \text{ metric tons} = 110{,}250 \text{ lb}, \quad (104)$$

$$\dot{M}_B = F_B/I_{sp} = 3.125 \times 10^4 \text{ gm/sec} \quad (105)$$

Case C:

$$F_c = 10^8 \text{ gm} = 100 \text{ metric tons} = 220{,}500 \text{ lb}, \quad (106)$$

$$\dot{M}_c = F_c/I_{sp} = 6.25 \times 10^4 \text{ gm/sec.} \quad (107)$$

B. Nomenclature Conventions

In Section III we let d_i and d_o denote, respectively, the inner and outer diameters of the solid wall of a single fuel element. Here, however, we are no longer interested in what happens at the outer edge of the solid wall. Hence there will be little danger of confusion if we change notation as follows: Let capital letters (R for radius and D for diameter) refer to fuel element dimensions, while lower case letters refer to the corresponding dimensions of a single bubble. The subscript o will refer to the bubble injection position, i.e., the outer surface of the liquid fuel annulus; similarly, the subscript i will refer to conditions at the liquid/gas interface, i.e., the outer surface of the central cavity. (The subscripts i and c are interchangeable, since it is assumed that the gas properties are uniform throughout the central cavity). Unsubscripted letters denote variables.

C. Fuel Element Geometry

In the new notation, according to Eqs. (76)-(68),

$$(R_o)_1 = 11.377 \text{ cm}, \tag{108}$$

$$(R_o)_2 = 3.9975 \text{ cm}, \tag{109}$$

$$(R_o)_3 = 1.286 \text{ cm}. \tag{110}$$

In order to determine the inner radii, $(R_i)_1$, $(R_i)_2$ and $(R_i)_3$, we must first decide how much of the 50% (intra-fuel element) void fraction is to be allocated to the central cavity and how much to the bubbles. On the one hand, it is desirable to maximize R_i, or at least keep the inner surface of the fuel annulus from being too near the axis, for otherwise the angular velocity required to achieve a specified centrifugal acceleration becomes excessive. On the other hand, it is obviously desirable to maximize the aggregate volume, V_b, of the bubbles in the fuel at any instant. The maximum permissible value of the ratio

$$\nu_b \equiv \frac{V_b}{V_f + V_b}, \tag{111}$$

of aggregate bubble volume to combined liquid fuel and aggregate bubble volumes is, however, fixed by another consideration. R. W. Bussard (5) cites a probable practical limit for this ratio of 0.3 to 0.4, if one wishes to avoid the extreme situation where the ligaments of liquid connecting intra-bubble regions break, so that the system is reduced to a collection of liquid droplets suspended in

the gas stream. In such a case small fuel droplets will tend to be swept out with the gas flow and the loss rate may be excessive, unless an additional separation stage is introduced.*

Actually, it will prove expedient to specify the spacings between bubbles (as functions of bubble size and depth). This, in turn, serves to fix ν_b uniquely. Nevertheless, it is necessary to keep in mind the limitation cited above when choosing the bubble spacings. That is, the spacings must be selected in such a way that ν_b does not exceed about 0.3.

Consistent with the particular choice of spacings which will be made below, it is necessary to assume that

$$\nu_b = 0.161 \tag{112}$$

This means that

$$V_b = \frac{.161}{.839} V_f = 0.192\ V_f \tag{113}$$

Since half the volume, V, within each fuel element consists of liquid fuel and the rest hydrogen (recall that the fuel element void fraction, $\nu \equiv (V - V_f)/V$, has been taken to be 50%), this implies the following apportionment of volumes:

---

* Professor R. Shinnar (6) has proposed a "mist core reactor" based upon this principle, which holds some promise of greater thrust levels than those possible with a liquid core reactor based on bubbles. The question of what would be the performance degradation (if any) which results from the mechanical complexity introduced by a subcritical centrifugal separator distinct from the reactor core is yet to be investigated.

$$V_f = V/2 , \tag{114}$$

$$V_b = 0.0959\ V, \tag{115}$$

$$V_{cavity} = V - V_f - V_b = 0.404\ V. \tag{116}$$

R_i is now fixed, since, by Eq. (116)

$$\pi R_i^2 = 0.404\, \pi\, R_o^2 \tag{117}$$

or

$$R_i = 0.636 R_o . \tag{118}$$

Thus

$$(R_i)_1 = 7.23\ cm, \tag{119}$$

$$(R_i)_2 = 2.54\ cm, \tag{120}$$

$$(R_i)_3 = 0.817\ cm \tag{121}$$

D. Bubble Shape, Velocity and Distribution

At this point it would be well to re-emphasize that all calculations are based on the assumption of steady-state operation. Investigation of the various types of transient behavior manifested in a liquid core reactor are beyond the scope of this simplified feasibility study.

In attempting to postulate a reasonable physical model for the bubbles in the core, it is important to realize that, since we wish to maximize the propellant flow rate (in order to maximize the thrust), we must deal with

"large" bubbles. More precisely, our attention must be confined to bubbles of very high Reynolds number. This implies that the shape of each bubble is approximately a spherical cap, and not a sphere (nor even an oblate spheroid). Hence the formulas of Stokes*, Hadamard and Rybczynsky** and Chao (8), all of which apply only to perfect spheres, are inapplicable. The Stokes formula is valid for a bubble whose Reynolds number is small compared with unity and indeed so small that the interface behaves like a solid wall; it gives the terminal velocity as proportional to gr^2. The Hadamard-Rybczynsky formula also applies only to the case where $Re \ll 1$, but takes into account the mobility of the interface; it gives a terminal velocity 50% greater than that given by the Stokes formula, the functional dependence being essentially the same. The Chao formula holds for bubbles whose Reynolds number is large compared with unity, but not so large that distortion of the spherical shape occurs; it takes into account the internal (gas) circulation and resembles the Hadamard-Rybczynsky formula except for a correction which depends on the Reynolds number.

It has been found experimentally that all bubbles of sufficiently high Reynolds number are very nearly spherical caps (see Figure 9). Actually, the downstream boundary tends to be slightly concave "downward" or irregular rather than just flat, but this refinement will

---

* See any standard work on hydrodynamics, e.g., Lamb (7), pp. 598-599.

** See Lamb, op. cit., pp. 600-601

be neglected. Taylor and Davies (9) have shown that the terminal velocity of a spherical cap bubble is

$$u = \frac{2}{3}\sqrt{gr}\ , \tag{122}$$

where r is the radius of curvature of the bubble. Note that the size- and accelerating field-dependences are quite different from those which prevail for spherical bubbles. Moreover, the divergence from sphericity, quite apart from its effect upon the velocity, also has non-negligible ramifications.

Defining the thickness, b, and the half-angle subtended, Θ, as shown in Figure 10, we see that

$$b = r\,(1 - \cos\Theta)\,. \tag{123}$$

Now, it is experimentally observed that all spherical cap bubbles are geometrically similar. In particular, it has been found that

$$\Theta \approx 52^{\circ}, \tag{124}$$

independent of r. While this is perhaps intuitively strange, it is nevertheless certainly a convenient fact. Thus we have

$$b = r\,(1 - \cos 52^{\circ}) = 0.384\ r\,. \tag{125}$$

It is now a simple matter to calculate the volume, v, of a bubble:

$$v = \int_{r-b}^{r} (r^2 - x^2)\,dx = \pi\left[r^2x - \frac{x^3}{3}\right]_{r-b}^{r}$$

$$= \pi\left\{\left(r^3 - \frac{r^3}{3}\right) - \left[r^2(r-b) - \frac{(r-b)^3}{3}\right]\right\}$$

$$= \pi\left(rb^2 - \frac{b^3}{3}\right). \qquad (126)$$

Substitution of Eq. (125) into Eq. (126) gives

$$v = 0.405\, r^3. \qquad (127)$$

The area of a spherical cap bubble is obtained as follows:

$$a_{cap} = \int_0^{2\pi}\int_0^{\theta} r^2 \sin\theta\, d\theta\, d\phi = 2\pi r^2 \int_0^{52^\circ} \sin\theta\, d\theta$$

$$= 2\pi r^2 (1-\cos 52^\circ) = 2\pi rb$$

$$= 0.769\,\pi r^2, \qquad (128)$$

$$a_{bottom} = \pi r^2 \sin^2\theta = 0.621\,\pi\, r^2. \qquad (129)$$

Thus

$$a = a_{cap} + a_{bottom} = 1.390\,\pi r^2$$

$$= 4.376\ r^2. \qquad (130)$$

The "equivalent radius", defined as the radius of a sphere of volume v, is then

$$r_e = \left[\frac{(3)(0.405)}{4}\right]^{1/3} r = 0.459\ r. \qquad (131)$$

For the sake of simplicity, we will assume that all the bubbles in the core are neatly arrayed in a "locally tetragonal" lattice. Let the center-to-center <u>lateral</u> separation

distance at station i be

$$s_i^{lat} = 2.01\, r_i \sin 52^o = 1.58\, r_i \,. \qquad (132)$$

This spacing is designated as "lateral" in order to indicate that it is assumed to be the same in the axial as in the circumferential direction. Clearly, this distance increases linearly with R. Thus, in general,

$$s^{lat} = 1.58\, r_i \left(\frac{R}{R_i}\right) \,. \qquad (133)$$

The maximum lateral separation occurs, of course, at injection:

$$s_o^{lat} = 1.58\, r_i \left(\frac{R_o}{R_i}\right) = 2.49\, r_i \,, \qquad (134)$$

where use has been made of Eq. (118).

The radial center-to-center separation at station i is assumed to be

$$s_i^{rad} = 1.26\, b = 0.461\, r_i \qquad (135)$$

where use has been made of Eq. (125). This too is a function of R, because the bubble terminal velocity varies (nonlinearly) with R. s_o^{rad} will be calculated later. Figure 10 is a schematic representation of the postulated bubble distribution. The foregoing assumptions, while somewhat arbitrary, nevertheless arise rather naturally from an attempt to minimize bubble interaction (e.g., coalescence of two or more bubbles) without resorting to severe depopulation and without making impossible demands on the bubble frequency.

Note that r_i (and therefore also r_o) are now really fixed, since we have chosen to specify both the aggregate bubble volume, V_b, and the spacing of the bubbles (the latter as functions of r_i). It is instructive, however, to consider r_i as a parameter or as an independent variable for the time being, especially since there is a certain degree of arbitrariness in the choices represented by Eqs. (114), (131) and (134). In this way it will be possible to plot the rotational frequency, ν, and the nondimensionalized acceleration, $\mathcal{n}$, of the fuel annulus vs. r_i for different cases of interest. Such curves will prove very useful. Later we will check to see that our particular choice of r_i is indeed compatible with Eq. (115) and the postulated spacings.

Let the fuel annulus thickness (i.e., the bubble path length*) be denoted by

$$R_o^* \equiv R_o - R_i \,, \tag{136}$$

and let

$$R^* \equiv R - R_i \tag{137}$$

denote the (variable) depth in the liquid fuel. In effect, then, we have assumed that the bubbles are confined to separate non-interacting radial stream tubes or "channels" of length R_o^* and of radius which varies from a minimum of

---

* The assumption that the bubble paths are rectilinear relative to the liquid, rather than helical or zig-zag, is implicit .

$r_o \sin\theta = 0.788\ r_o$ at injection to a maximum of

$r_i \sin\theta = 0.788\ r_i$ at emergence.

The bubbles are formed with a constant frequency, φ. This means that at any fixed depth R_j^* $(0 \leq R_j^* \leq R_o^*)$, bubbles ascend past this depth per second in each channel. Clearly,

$$\varphi = \frac{u_i}{s_i^{rad}} \quad . \tag{138}$$

The total number of channels in a single fuel element is

$$C = \left(\frac{2\pi R_i}{s_i^{lat}}\right)\left(\frac{H}{s_i^{lat}}\right) = \frac{2\pi R_i H}{2.51 r_i^2} \tag{139}$$

$$= \frac{1260\ R_i}{r_i^2} \ ,$$

where the value of the fuel element length has been substituted from Eq. (86) and use has been made of Eq. (132). Thus the number of channels per square centimeter of fuel element wall area (inner surface) is

$$\frac{C}{A_o} = \frac{C}{2\pi R_o H} = 0.254\ r_i^{-2} \ , \tag{140}$$

where use has been made of Eq. (118)

E. Centrifugal Acceleration and Bubble Size

Let us focus our attention now upon station i, where the bubbles emerge into the central cavity. Recalling that the subscripts c and i are interchangeable (because the central cavity is assumed to be homogeneous), we may substitute

Eqs. (97), (98) and (100) into the perfect gas law to obtain:

$$\rho_i = \frac{\mathfrak{M}_i \, p_i}{\mathfrak{R} \, T_i} = \frac{(1.465)(1.013)(10^7)}{(8.31)(10^7)(43000)}$$

$$= 4.16 \times 10^{-5} \text{ gm/cm}^3. \qquad (141)$$

Using Eqs. (127) and (140), we see that each bubble crossing station i has mass

$$m_i = v_i \rho_i = 0.405 \; r_i^3 \rho_i = (1.68)(10^{-5}) \; r_i^3. \qquad (142)$$

The mass flow rate of gas in a single fuel element is

$$\dot{M} = m_i \, C\varphi$$

$$= (1.68 \times 10^{-5} \; r_i^3)\left(\frac{1260 \; R_i}{r_i^2}\right)\left(\frac{u_i}{s_i^{rad}}\right) \qquad (143)$$

where use has been made of Eqs. (142), (139) and (135). Substituting Eq. (122) into Eq. (143) gives

$$\dot{M} = 0.0307 \; R_i g_i^{1/2} r_i^{1/2}. \qquad (144)$$

But

$$g_i = \omega^2 R_i = 4\pi^2 \nu^2 R_i, \qquad (145)$$

where ω is the angular velocity and ν is the rotational frequency. Substituting Eq. (145) into Eq. (144) gives

$$\dot{M} = 0.193 \nu R_i^{3/2} r_i^{1/2}. \qquad (146)$$

Eliminating $\dot{M}$ between Eq. (146) and the following obvious relation:

$$\dot{M} = \dot{M}_{tot}/N \qquad (147)$$

and solving for ν, we have

$$\nu = \frac{5.19\ \dot{M}_{tot}}{N R_i^{3/2} r_i^{1/2}} \quad \text{rev/sec}$$

$$= \frac{311\ \dot{M}_{tot}}{N R_i^{3/2} r_i^{1/2}} \quad \text{rev/min}. \qquad (148)$$

Now

$$g_{max} \equiv g_o = 4\pi^2 \nu^2 R_o$$

$$= \frac{4\pi^2 \nu^2 R_i}{0.636} = \frac{1670\ \dot{M}^2_{tot}}{N^2 R_i^2 r_i}. \qquad (149)$$

We now define

$$\eta_o \equiv \text{maximum number of g's acceleration}$$

$$\equiv g_o/980.7$$

$$\equiv \frac{1.70\ \dot{M}^2_{tot}}{N^2 R_i^2 r_i}. \qquad (150)$$

η_{min} ($\equiv \eta_i$) and g_{min} ($\equiv g_i$) are, of course, just 0.636 times respective minimum values (cf. Eq. (118)). Figure 11 plots ν vs. r_i for different core matrix geometries (Cases 1, 2 and 3) and different thrust levels (Cases A, B and C) of interest. Figure 12 plots η_o vs. r_i for the same nine cases.

The dashed parts on the right-hand side of the curves in Figures 11 and 12 represent "forbidden zones",

corresponding to conditions where the bubble size is too large for the specified fuel depth. Of course heat transfer considerations must really also be taken into account in the definition of such zones. Until we have actually carried out the necessary heat transfer calculation (see below), it will suffice to adopt the following criterion as the definition of these forbidden zones:

$$(r_i)_{\text{forbidden}} > R_o^* / 5 . \qquad (151)$$

Although perhaps somewhat arbitrary, this is not at all unreasonable; it means that the maximum radius of curvature of a (spherical cap) bubble must not be permitted to exceed 20% of the path length, and thus, more significantly, that the maximum bubble thickness must be less than 7.69% of the path length. In other words, we had better allow room for at least 10 bubbles per channel at any instant. This is only about one order of magnitude below the point at which we have gas jets rather than bubble streams in the core. Moreover, as we will see later, in the range of practical interest the maximum size bubble which can be "fully heated" turns out to be just about $R_o^*/5$.

There is an additional criterion which must be satisfied: The stress σ on the solid wall of a fuel element due to the centrifugal force upon the fuel must be kept below some definite value σ_{max} which is characteristic of the wall material. Since the fuel element walls are

assumed to consist of ZrC and are cooled by transpiration of relatively cold hydrogen gas, it appears reasonable to postulate that

$$\sigma_{max} \approx 10{,}000 \text{ psi} = 6.90 \times 10^8 \text{ dynes/cm}^2. \quad (152)$$

This is probably a slightly conservative value. The mean centrifugal acceleration is

$$g_m = 0.8178\, g_o , \quad (153)$$

since $g_i = 0.63565\, g_o$. Thus we set

$$\sigma_{max} = 6.90 \times 10^8 = \frac{M_f g_m}{A_o} = \frac{(1.04)(10^8)(0.636) g_{o_{max}}}{2\pi R_o H N}$$

$$= \frac{1.303 \times 10^7 \mathfrak{N}_{o_{max}}}{R_i N} , \quad (154)$$

where use has been made of Eqs. (66), (86), and (118). Solving for $\mathfrak{N}_{o_{max}}$, we obtain

$$\mathfrak{N}_{o_{max}} = 52.9\, R_i N . \quad (155)$$

Hence, for core matrices 1, 2 and 3 we have, respectively,

$$(\mathfrak{N}_{o_{max}})_1 = 3.89 \times 10^5, \quad (156)$$

$$(\mathfrak{N}_{o_{max}})_2 = 1.37 \times 10^5, \quad (157)$$

$$(\mathfrak{N}_{o_{max}})_3 = 4.40 \times 10^4. \quad (158)$$

The forbidden zones where $\mathfrak{N}_o > \mathfrak{N}_{o_{max}}$ appear as dotted portions on the left-hand side of the curves in Figures 11 and 12. The two principal considerations on which to base a

design-point selection are as follows:

A. The rotation frequency must be as low as possible. Indeed, the necessity for any "clockwork" at all inside the core is bad enough, but the mechanical problems must certainly be kept to a minimum. (It is important, however, not to exaggerate this problem; the outer surfaces of the solid moving parts are relatively cool, so the engineering difficulties which may be encountered will more closely resemble those of a motor than those of a turbine). All this presupposes, of course, that centrifugation of the fuel is achieved by the straightforward means of driving the entire array of fuel elements as a train of tubular gears. However, at least two other schemes are conceivable, viz., tangential gas injection to drive each fuel annulus and an arrangement of crossed electric and magnetic fields resembling a homopolar motor whose armature is the liquid fuel itself. The former entails very tricky fabrication problems, but otherwise seems quite feasible, and the latter suffers from a host of serious problems, chief of which involve the electrical power requirement and the introduction into the axial region of each fuel element a vapor jet or plasma jet electrode (a solid one would of course defeat the whole purpose of a

liquid core reactor).

B. The bubble size should be smaller than that at which hydrodynamic instabilities (leading to breakup) set in. This critical size depends on g and will be estimated below.

On the basis of these qualitative considerations let us tentatively single out for further investigation the following model system (represented as a small circle in Figure 11 and in Figure 12):

$$N = 1017 \quad \text{(Case 2)}, \tag{159}$$

$$R_i = 2.5408 \text{ cm}, \tag{160}$$

$$R_o^* = 1.4567 \text{ cm}, \tag{161}$$

$$F = 5 \times 10^7 \text{ gm} = 110{,}250 \text{ lb}, \quad \text{(Case B)}, \tag{162}$$

$$r_i = 0.2 \text{ cm}, \tag{163}$$

$$\mathcal{R}_o = 1243, \tag{164}$$

$$g_o = 1.22 \times 10^6 \text{ cm/sec}^2 \tag{165}$$

$$\nu = 88.0 \text{ rev/sec} = 5280 \text{ rev/min} \tag{166}$$

F. Conditions At Bubble Injection

Let us now consider station o. Before we can calculate p_o and ρ_o, it is necessary to know T_o. Strictly speaking, T_o must be determined from heat transfer considerations. In particular, if it is assumed that the gas enters the porous wall of the fuel element at slightly

above the critical temperature (e.g., at about 50°K) or at some higher temperature to which it has been "pre-heated" by gamma radiation and conduction during the time it takes to flow from the vicinity to the pump to the pre-injection manifold, then the temperature rise across the wall may easily be calculated, since the flow rate is fixed by the thrust requirement. In Paragraph E of Section III, however, we have assumed (pending a thermal stress analysis) that the wall thickness, t, is given by Eq. (79). Since T_o depends on t (among other things), we must defer calculation of the former until after we have actually calculated the latter. For the time being (and subject to later re-examination), let us therefore postulate the following arbitrary value:

$$T_o = 800^\circ K. \qquad (167)$$

We already know everything about a single bubble at station i: p_i, T_i and ρ_i are given by Eqs. (98), (97), and (141), respectively, and r_i is given by Eq. (163). We must now find p_o, ρ_o and r_o. By the time a bubble reaches the inner surface of the fuel annulus, it has already undergone considerable expansion. This expansion is due to the temperature increase as the bubble "ascends", and also to the decrease in hydrostatic pressure due to the centrifugal field. Neglecting the hydrostatic pressure drop across the radius of the central gas cavity and assuming the liquid fuel density to be uniform (both good assumptions),

we see that

$$p_o = p_i + p_h , \tag{168}$$

where

$$p_h = \rho_f' \int_{R_i}^{R_o} g \, dR = \rho_f' \omega^2 \int_{R_i}^{R_i \sqrt{\frac{V}{V_{cavity}}}} R \, dR$$

$$= \frac{1}{2} \rho_f' \omega^2 R_i^2 \left[\frac{V}{V_{cavity}} - 1 \right]$$

$$= \frac{1}{2} \rho_f' g_i R_i \left[\frac{V}{V_{cavity}} - 1 \right] , \tag{169}$$

where ρ_f' is the <u>effective</u> density of the liquid fuel (i.e., including the bubble population). Since the gas density is negligible compared with the fuel density, it follows that

$$\rho_f' = (1 - \gamma_b) \rho_f = 5.730 \text{ gm/cm}^3 , \tag{170}$$

where use has been made of Eqs. (65) and (112). Noting that $g_i = (R_i/R_o) g_o$ and substituting Eqs. (116), (170), (165), (118) and (120) into Eq. (169), we obtain

$$p_h = 8.35 \times 10^6 \text{ dynes/cm}^2 = 8.2 \text{ atm.} \tag{171}$$

Note that the "effective" acceleration, defined as

$$g_m = \frac{p_h}{\rho_f' R_o^*} , \tag{172}$$

is identical with the mean acceleration given by Eq. (153), viz.,

$$g_m = 9.98 \times 10^5 \text{ cm/sec}^2 \tag{173}$$

Substituting Eq. (98) and (171) into Eq. (168) gives

$$p_o = 1.848 \times 10^7 \text{ dynes/cm}^2 = 18.2 \text{ atm} = 267.5 \text{ psi} \tag{174}$$

This is a moderately high pressure for a twelve foot diameter structure to be capable of withstanding. Recalling, however, that the pressure shell, which is considered to be identical with the beryllium reflector, is 21 cm (= 8.26") thick, it is readily seen that the stress is quite tolerable.

From the perfect gas law we may now obtain ρ_o. Making use of Eqs. (167) and (174) and noting that for the cool gas $\mathcal{M}_o$ = 2.016 a.m.u., we have

$$\rho_o = \frac{p_o \mathcal{M}_o}{\mathcal{R} T_o} = 5.596 \times 10^{-4} \text{ gm/cm}^3. \tag{175}$$

Thus we see that

$$\frac{\rho_o}{\rho_i} = \frac{v_i}{v_o} = \frac{r_i^3}{r_o^3} = 13.47, \tag{176}$$

so

$$r_o = r_i/2.38 = 8.405 \times 10^{-2} \text{ cm}. \tag{177}$$

Substituting Eqs. (165) and (177) into Eq. (122) gives

$$u_o = 263 \text{ cm/sec}. \tag{178}$$

Similarly, we find that

$$u_o = \frac{2}{3}\sqrt{g_i r_i} = 262 \text{ cm/sec} \tag{179}$$

G. Bubble Population and Wall Porosity

Substituting Eqs. (179), (135) and (163) into Eq. (138) gives the bubble frequency as

$$\varphi = 2847 \text{ sec}^{-1} \tag{180}$$

But φ is a constant and therefore also given by

$$\varphi = \frac{u_o}{s_o^{rad}}$$

Substituting for u_o from Eq. (178) and solving for s_o^{rad}, we find

$$s_o^{rad} = 0.0749 \text{ cm.} \tag{182}$$

This compares with

$$s_i^{rad} = 0.0922 \text{ cm,} \tag{183}$$

where use has been made of Eqs. (163) and (135).

Substituting Eq. (163) into Eqs. (132) and (134), we find that

$$s_i^{lat} = 0.317 \text{ cm} \tag{184}$$

$$s_o^{lat} = 0.499 \text{ cm} \tag{185}$$

The lateral spacing varies linearly with R^*, but the radial spacing varies as $(R^* r)^{1/2}$; r in turn varies as $\rho^{-1/3}$ but ρ itself depends on two things: the local hydrostatic pressure (as determined from an equation similar to Eq. (169), since g is non-uniform), and also the local temperature, which has not yet been calculated. The simplest thing to do in a situation like this is to replace the actual s^{rad}- variation by a constant equal to the arithmetic mean of the extreme

values. Fortuitously, these extreme values, given by Eqs. (182) and (183), are quite close together, so our simplification does not introduce any large error. Thus we assume a uniform radial separation throughout the fuel annulus of

$$s_m^{rad} = 0.0836 \text{ cm}. \tag{186}$$

We may certainly do the same thing with s^{lat}, since it is a linear function. Thus we take

$$s_m^{lat} = 0.404 \text{ cm}. \tag{187}$$

The average number of bubbles inhabiting each channel at any instant is then just

$$\frac{R_o^*}{s_m^{rad}} = 17.4, \tag{188}$$

From Eq. (139) we find that there are

$$C = 80{,}000 \tag{189}$$

channels per fuel element. Hence, at any instant there are

$$y = \lceil C = 1.39 \times 10^6 \tag{190}$$

bubbles in each fuel element, and

$$Y = Ny = 1.417 \times 10^9 \tag{191}$$

bubbles in the entire core.

The mean volume of an individual bubble is

$$v_m = \frac{v_i}{2}\left(1 + \frac{v_o}{v_i}\right) = 1.739 \times 10^{-3} \text{ cm}^3, \tag{192}$$

where use has been made of Eqs. (127), (163) and (176). Thus the aggregate bubble volume within a single fuel

element is

$$V_b = v_m y = 2420 \text{ cm}^3. \tag{193}$$

Now the central gas cavity has a volume

$$V_{cavity} = \pi R_i^2 H = 10,200 \text{ cm}^3. \tag{194}$$

But according to Eqs. (115) and (116), it is necessary that

$$V_{cavity} = \frac{0.404}{0.0959} V_b = 4.21 V_b . \tag{199}$$

By substituting Eq. (193) into Eq. (199) it is immediately verified that, to within the accuracy of the foregoing calculations, Eq. (194) does indeed agree with Eq. (199). It was in order to ensure this agreement that we have specified the particular value of $\sqrt{}_b$ given by Eq. (112).

It would be interesting to know the size of the orifices at which the bubbles are formed and also the wall porosity. In order to calculate these quantities, however, it is necessary first to know such things as the surface tension and viscosity of the liquid fuel at the particular temperature prevailing at injection, as well as the relevant "bubble formation regime" (the particular relationship between bubble size and orifice size depends on the range in which φ lies). Since data of this sort are unavailable at the present time, it seems not unreasonable to postulate arbitrarily that, at the instant a bubble breaks away from the orifice, its diamter is just twice that of the

orifice. That is, we assume that, if d_o is the bubble "diameter" (i.e., lateral width) at the instant of breakoff, then

$$f \equiv \frac{d_o}{d_{orifice}} = \frac{r_o \sin}{r_{orifice}} = 2 . \qquad (200)$$

Then the wall porosity (based on its inner surface) is

$$\Pi = \frac{\pi (r_o \sin\theta)^2 \, C}{2\pi R_o H_f^{\,2} \, f^2} = \frac{r_o^2 \, \sin^2 52^o \, C}{8 \, R_o H}$$

$$= 0.0218. \qquad (201)$$

Taking into account the f-factor given by Eq. (200), we see that each orifice in the fuel element wall must have a diameter

$$d_{orifice} = r_o \sin 52^o = 6.623 \times 10^{-2} \text{ cm}$$

$$= 0.0331". \qquad (202)$$

According to Eq. (139), there are

$$\frac{C}{A_o} = 6.34 \qquad (203)$$

holes per square centimeter of wall (inner) surface, which means that the holes are spaced about 0.4 cm apart. Thus the fabrication of each fuel element entails drilling some 80,000 holes of 33 mil diameter through a ZrC tube whose wall thickness is about half a centimeter. This task does not seem to be unreasonable.

Defining u_m as the arithmetic mean of u_o and u_i, we see that the average residence time, τ, of a bubble within the fuel annulus is

$$\tau = \frac{R_o^*}{u_m} = \frac{1.456}{238} = 6.12 \times 10^{-3} \text{ sec.} \quad (204)$$

We next address ourselves to the question: Can we indeed attain the requisite temperature rise in the interior of a bubble within 6.12 milliseconds?

H. Heat Transfer: Conduction To The Interior of a Bubble

In order to ascertain whether or not temperature equilibration (between the bubbling gas and the ambient liquid fuel) is possible in the time available, it is necessary to make a number of simplifying assumptions, for otherwise the analysis would become too unwieldy. However, insofar as it is practical to do so, we will endeavor to avoid optimistic assumptions. First, let us take the shape of a bubble to be a sphere of radius $a \equiv r_e$, given by Eq. (131). Secondly, we will neglect the heat convection due to internal gas circulation, even though the vorticity is really not negligible. Thirdly, we assume that the liquid fuel annulus has a uniform temperature of

$$T_i = 4300^{\circ}\text{K.}^* \quad (205)$$

---

* See Footnote on page 5.

Another simplification is the following: We will divide the maximum fuel depth R_o^* into four equal segments. Each bubble successively traverses the corresponding four concentric regions. Defining ℓ as the radial distance measured inward from station o, then the four regions are designated as follows:

Region 01: Bounded by R_o ($\ell = o$) and R_1 ($\ell = \ell_1 = R_o^*/4 = 0.364$ cm),

Region 12: Bounded by R_1 and R_2 ($\ell = \ell_2 = R_o^*/2 = 0.728$ cm),

Region 23: Bounded by R_2 and R_3 ($\ell = \ell_3 = R_o^*/4 = 1.093$ cm),

Region 34: Bounded by R_3 and $R_4 = R_o^*$ ($\ell = \ell_4 = R_o^* = 1.457$ cm).

Midway between the boundaries of each region lie the surfaces:

$$\ell = \ell_{01} = 0.182 \text{ cm}, \tag{206}$$

$$\ell = \ell_{12} = 0.546 \text{ cm}, \tag{207}$$

$$\ell = \ell_{23} = 0.910 \text{ cm}, \tag{208}$$

$$\ell = \ell_{34} = 1.275 \text{ cm}. \tag{209}$$

Materials properties evaluated at each of these surfaces (and denoted by the corresponding subscripts, j(j+1), where j = 0, 1, 2, 3) will be assumed to apply uniformly throughout the respective Region j(j+1).

The entire problem is thus reduced to four interrelated (but simplified) time-dependent problems of heat conduction into a sphere. Given the liquid fuel temperature and the gas temperature at injection, as well

as the time for traversal of Region 01, we calculate the temperature at the center of a bubble at the end of this time. Then, taking the new center temperature as an initial value, we calculate the center temperature at the instant the bubble emerges from Region 12, and so on, until it arrives at station i.

It should be noted that the liquid fuel temperature is assumed to be always the same as that at the surface of every bubble. In other words, we ignore here the question of heat transfer across the thermal boundary layer of a bubble. This matter requires further investigation and will be considered separately below.

Let

$$\tau \equiv \text{time}, \tag{210}$$

$$a \equiv r_e = \text{radius of spherical bubble}, \tag{211}$$

$$r \equiv \text{variable radial distance from the center of a spherical bubble}, \tag{212}$$

$$\alpha \equiv \text{thermal diffusivity of the gas}, \tag{213}$$

$$\vartheta \equiv T_{interior} - T_{center}^{initial}, \text{ where}$$

$$T_{interior} = T_{interior}(r, \tau), \tag{214}$$

$$\vartheta_c \equiv T_{center} - T_{center}^{initial} \tag{215}$$

$$V \equiv T_{surface} - T_{center}^{initial} \tag{216}$$

The solution of the heat conduction equation under the pertinent boundary conditions is given by Carslaw and

Jaeger (10) as:

$$v = V + \frac{2aV}{\pi r}\sum_{n=1}^{\infty}\frac{(-1)^n}{n}\sin\frac{n\pi r}{a}\,e^{-\alpha n^2\pi^2\tau/a^2}$$

$$= \frac{aV}{r}\sum_{n=0}^{\infty}\left[\operatorname{erfc}\frac{(2n+1)a-r}{2(\alpha\tau)^{1/2}} - \operatorname{erfc}\frac{(2n+1)a+r}{2(\alpha\tau)^{1/2}}\right], \tag{217}$$

where erfc is the complementary error function:

$$\operatorname{erfc} x \equiv \frac{2}{\sqrt{\pi}}\int_x^{\infty} e^{-\xi^2}\,d\xi\,. \tag{218}$$

v_c is given by the limit as $r \to 0$ of Eq. (217):

$$v_c = V + 2V\sum_{n=1}^{\infty}(-1)^n e^{-\alpha n^2\pi^2\tau/a^2}$$

$$= \frac{aV}{(\pi\alpha\tau)^{1/2}}\sum_{n=0}^{\infty} e^{-(2n+1)^2a^2/4\alpha\tau}\,. \tag{219}$$

Figure 13 presents a plot of v_c/V vs. $\alpha\tau/a^2$, as computed from Eq. (219).

We begin our "four region calculation" as follows: The actual variation of u with R^*, which is not a strong variation, as may readily be seen by comparison of Eqs. (178) and (179), is replaced by a linear function of λ:

$$u = 213.47 + 33.69\ s \text{ cm/sec}, \tag{220}$$

This introduces only relatively small errors but vastly simplifies the computational procedure. Thus we have:

$$u_{01} = 219.6 \text{ cm/sec}, \tag{221}$$

$$u_{12} = 231.9 \text{ cm/sec}, \tag{222}$$

$$u_{23} = 244.1 \text{ cm/sec}, \tag{223}$$

$$u_{34} = 256.5 \text{ cm/sec}. \tag{224}$$

The corresponding traversal times are given by

$$\tau_{j(j+1)} = \frac{\Delta \ell}{u_{j(j+1)}} = \frac{R_o^*}{4\, u_{j(j+1)}}. \tag{225}$$

Thus

$$\tau_{01} = 1.658 \times 10^{-3} \text{ sec}, \tag{226}$$

$$\tau_{12} = 1.570 \times 10^{-3} \text{ sec}, \tag{227}$$

$$\tau_{23} = 1.492 \times 10^{-3} \text{ sec}, \tag{228}$$

$$\tau_{34} = 1.420 \times 10^{-3} \text{ sec}. \tag{229}$$

The time for traversal of the entire annulus adds up to

$$\tau_{tot} = 6.140 \times 10^{-3} \text{ sec}. \tag{230}$$

In order to circumvent a tedious iteration procedure, we now introduce an additional simplifying assumption: We postulate that the center temperature increases linearly with ℓ, from $T_o = 800^oK$ to $T_i = 4300^oK$, according to the formula:

$$T = 800 + 2402\,\nu . \tag{231}$$

As we will see later, this is a rather pessimistic assumption. (The "actual" temperature will turn out to be greater than that given by Eq. (231) at every point along the bubble path). Nevertheless, assuming this conservative temperature law, we have:

$$T_{01} = 1237^{\circ}K, \tag{232}$$

$$T_{12} = 2112^{\circ}K, \tag{233}$$

$$T_{23} = 2987^{\circ}K, \tag{234}$$

$$T_{34} = 3862^{\circ}K . \tag{235}$$

The hydrostatic pressure due to centrifugal acceleration of the fuel varies, of course, with position. It is given by

$$p_h = \rho_f' \omega^2 \int_{R_i}^{R_o - a} R\,dR = 2\pi^2 \nu^2 \rho_f' \left[(R_o - a)^2 - R_i^2 \right] . \tag{236}$$

The local pressure is then

$$p = p_i + p_h . \tag{237}$$

In this manner we find that

$$p_{01} = 1.723 \times 10^7 \text{ dynes/cm}^2 = 250 \text{ psi}, \tag{238}$$

$$p_{12} = 1.491 \times 10^7 \text{ dynes/cm}^2 = 216 \text{ psi}, \tag{239}$$

$$p_{23} = 1.282 \times 10^7 \text{ dynes/cm}^2 = 186 \text{ psi}, \tag{240}$$

$$p_{34} = 1.097 \times 10^7 \text{ dynes/cm}^2 = 159 \text{ psi}. \tag{241}$$

The next thing we must know is the molecular mass $\mathfrak{M}$

corresponding to each of the four sets of temperatures and pressures. For this we refer to Figure 10 of the Technical Note by C. R. King (4). We find that

$$\mathfrak{M}_{01} = \mathfrak{M}_{12} = 2.016 \text{ a.m.u.}, \tag{242}$$

$$\mathfrak{M}_{23} = 1.97 \text{ a.m.u.}, \tag{243}$$

$$\mathfrak{M}_{34} = 1.695 \text{ a.m.u.} \tag{244}$$

From the perfect gas law we may now determine the densities. The results are:

$$\rho_{01} = 3.375 \times 10^{-4} \text{ gm/cm}^3, \tag{245}$$

$$\rho_{12} = 1.709 \times 10^{-4} \text{ gm/cm}^3, \tag{246}$$

$$\rho_{23} = 1.017 \times 10^{-4} \text{ gm/cm}^3, \tag{247}$$

$$\rho_{34} = 5.78 \times 10^{-5} \text{ gm/cm}^3. \tag{248}$$

Now, the radii of curvature of spherical cap bubbles are determined from the relation:

$$r = \left(\frac{\rho_o}{\rho}\right)^{1/3} r_o , \tag{249}$$

where ρ_o and r_o are given by Eqs. (175) and (177), respectively. Thus, by virtue of Eq. (131), the radii of the equivalent spherical bubbles are given by

$$a \equiv r_e = 0.4589\, r_o \left(\frac{\rho_o}{\rho}\right)^{1/3} . \tag{250}$$

From Eq. (250) we find:

$$a_{01} = 4.565 \times 10^{-2} \text{ cm}, \tag{251}$$

$$a_{12} = 5.725 \times 10^{-2} \text{ cm}, \tag{252}$$

$$a_{23} = 6.804 \times 10^{-2} \text{ cm}, \tag{253}$$

$$a_{34} = 8.210 \times 10^{-2} \text{ cm}. \tag{254}$$

From Figure 2 of King's paper (4) we find:

$$c_{p_{01}} = 4.0 \text{ cal/gm} - {}^{\circ}\text{K}, \tag{255}$$

$$c_{p_{12}} = 4.5 \text{ cal/gm} - {}^{\circ}\text{K}, \tag{256}$$

$$c_{p_{23}} = 8.0 \text{ cal/gm} - {}^{\circ}\text{K}, \tag{257}$$

$$c_{p_{34}} = 23.2 \text{ cal/gm} - {}^{\circ}\text{K}, \tag{258}$$

and from Figure 10 of King's paper (4) we determine the thermal conductivities:

$$k_{01} = 1.0 \times 10^{-3} \text{ cal/sec-cm-}{}^{\circ}\text{K}, \tag{259}$$

$$k_{12} = 1.8 \times 10^{-3} \text{ cal/sec-cm-}{}^{\circ}\text{K}, \tag{260}$$

$$k_{23} = 3.8 \times 10^{-3} \text{ cal/sec-cm-}{}^{\circ}\text{K}, \tag{261}$$

$$k_{34} = 11.4 \times 10^{-3} \text{ cal/sec-cm-}{}^{\circ}\text{K}. \tag{262}$$

Combining the foregoing data, we obtain values for the parameter

$$\frac{\alpha\tau}{a^2} = \frac{k\tau}{\rho c_p a^2} \tag{263}$$

as follows:

$$(\alpha\tau/a^2)_{01} = 0.590, \tag{264}$$

$$(\alpha\tau/a^2)_{12} = 1.122, \tag{265}$$

$$(\alpha\tau/a^2)_{23} = 1.503, \tag{266}$$

$$(\alpha\tau/a^2)_{24} = 1.791. \tag{267}$$

Corresponding to these values we find from Figure 13:

$$(\upsilon_c/V)_{01} = 0.9944, \tag{268}$$

$$\left(\frac{\upsilon_c}{V}\right)_{12} \approx \left(\frac{\upsilon_c}{V}\right)_{23} \approx \left(\frac{\upsilon_c}{V}\right)_{34} \approx 1.0000. \tag{269}$$

Thus, by the time a bubble has traversed Region 01, its center temperature has already reached

$$T_1 = 800+(0.9944)(4300-800) = 4280.4^{\circ}K$$

From Eq. (269) it is evident that a bubble achieves essentially the ambient liquid fuel temperature well before it has traversed Region 12. Thus we see that there should be no difficulty at all in heating up the gas in the time (or path length) available. Note, incidentally, that our earlier claim that the center temperature of a bubble exceeds that given by Eq. (231) at every point along its path is indeed verified.

There are at least two factors which make the heating process an even more efficient one than that considered above. First, the bubbles are spherical caps rather than spheres. The extra surface area should improve the heat transfer noticeably. Secondly, there is the convection due to the vorticity of the gas within each bubble. This has been neglected in tne foregoing analysis, but its effect should be very pronounced. Assuming that the gas near the interface of a bubble moves with a velocity

of the same order of magnitude as the bubble's local "terminal" velocity (which is certainly true; see e.g., Chao (8)), then it follows that during the time a bubble takes to traverse the liquid, this outer layer of gas will move along the boundary (and along the thickness, b) of the bubble a total distance of the order of $R_o^* = 1.456$ cm. But this is equivalent to many circuits within the bubble, so we conclude that convection must indeed by extremely important.

I. Heat Transfer Across the Thermal Boundary Layer

The next question is that of heat transmission across the thermal boundary layer. In particular, we wish to inquire whether or not heat can cross this boundary layer at a rate sufficient to support the magnitude of internal temperature rise previously calculated.

The required rate of heat transfer is maximum in Region 01, the center temperature rise there being

$$T_{01} = 3480.4^{\circ}K \qquad (270)$$

as compared with $19.6^{\circ}K$ for Region 12 and essentially zero for Regions 23 and 34. Assuming that the rate of fuel evaporation into a bubble is negligible (a matter which will be investigated below), the mass, m, of a bubble remains constant. Hence, making use of Eqs. (142), (163), (255), (270) and (226), we find that the maximum

rate at which heat must be transferred to a single bubble is

$$Q_{max} = \frac{m_i c_{p_{01}} \Delta T_{01}}{\tau_{01}} = 1.13 \text{ cal/sec}, \qquad (271)$$

This magnitude is perhaps better appreciated intuitively when expressed in terms of a maximum heat transfer rate per unit area. Substituting Eq. (131) into Eq. (130), we see that the total surface area of a spherical cap bubble in Region 01 is

$$a \equiv \text{area} = 20.73\, a_{01}^2 \text{ cm}^2. \qquad (272)$$

Thus, making use of Eq. (251), we have

$$a = 0.0432 \text{ cm}^2, \qquad (273)$$

so

$$q_{max} \equiv \frac{Q_{max}}{a} = 26.19 \text{ cal/sec-cm}^2$$

$$= 109.6 \text{ watts/cm}^2 = 3.47 \times 10^5 \text{ Btu/hr - ft}^2. \qquad (274)$$

The rate at which heat is transferred across the thermal boundary layer to the surface of a <u>spherical</u> bubble of high Reynolds number (i.e., $Re \gg 1$), has been derived by S. T. Nelson (11). The result is

$$Q = \rho_f c_{p_f} \Delta T_{01} \sqrt{6\pi \alpha_f u_{01} a_{01}^3} \text{ J}, \qquad (275)$$

where α_f is the thermal diffusivity of the liquid fuel:

$$\alpha_f \equiv \frac{k_f}{\rho_f c_{p_f}}, \qquad (276)$$

and

$$J \equiv \int_0^{\pi} \frac{\sin^3\theta \left[1 - \frac{K\sqrt{2+\cos\theta}}{1+\cos\theta}\right] d\theta}{\sqrt{N^2 - K\left[(2+\cos\theta)^{3/2}\left(\frac{4}{5}\cos\theta - 2\right) - \frac{6}{5}(3)^{3/2}\right]}} \quad (277)$$

where

$$N^2 \equiv \frac{2}{3} - \cos\theta + \frac{\cos^3\theta}{3} \quad (278)$$

and

$$K \equiv \frac{4 \text{ ierfc } 0}{3\sqrt{Re}} , \quad (279)$$

where ierfc is the first integral of the complementary error function and the Reynolds number, Re, is based on the bubble diameter, $2a_{01}$.

For our purposes it will be sufficient to approximate J by the simple expedient of invoking the mean value theorem of the integral calculus, but with the actual mean value of the integrand, $\overline{f(\theta)}$, replaced by its value at $\theta = \frac{\pi}{2}$. (The integrand, $f(\theta)$, of J vanishes at both endpoints of the interval of integration and, as we will see below, is 1.15 at $\pi/2$). Thus we write:

$$J = \pi \overline{f(\theta)} \approx \pi f\left(\frac{\pi}{2}\right) . \quad (280)$$

In order to evaluate the Reynolds number we must know the viscosity, μ_f , of the liquid fuel. For want of experimental data, let us simply assume that

$$\mu_f \approx 10^{-2} \text{ poise.} \tag{281}$$

This value is typical of many fused metals and other liquids (including water). In order to properly compare the value of Q obtained from Eq. (272) with the value of Q_{max} given by Eq. (271), it is necessary to evaluate all the variables at $\Delta = \Delta_{01}$. Making use of Eqs. (251), (65), (221) and (281) we find that

$$\text{Re} \equiv \frac{2a_{01}\rho_f u_{01}}{\mu_f} = 13{,}700. \tag{282}$$

Now

$$\text{ierfc } 0 = 0.564, \tag{283}$$

so that

$$K = 6.42 \times 10^{-3}. \tag{284}$$

Substitution of this value for K and $\pi/2$ for θ in Eqs. (277) (280) gives

$$J \approx 1.15\pi = 3.62 \tag{285}$$

Making use of Eqs. (276) and (285), we can write Eq. (275) as

$$Q = 3.62\, a_{01}\Delta T_{01}\sqrt{6\pi k_f \rho_f c_{p_f} u_{01} a_{01}} \,. \tag{286}$$

The only unknowns in Eq. (286) are k_f and c_{p_f}. Since the dilution ratio for the sample case is taken to be 500 (cf. Eq. (58)), we may expect that the thermal conductivity and specific heat at constant pressure of the fuel are very nearly the same as the respective values for pure ZrC. The former is given in the Reactor Handbook (12) as

$$k_f = 4.9 \times 10^{-2} \text{ cal/sec-cm-}^{\circ}\text{K} \qquad (287)$$

and the latter is given in the Janaf Tables (13) (corresponding to a temperature of 4300°K) as

$$c_{p_f} = 15 \text{ cal/mole - }^{\circ}\text{K} = 0.1452 \text{ cal/gm - }^{\circ}\text{K} \qquad (288)$$

Making use of these values, we find that

$$Q = 1741 \text{ cal/sec.} \qquad (289)$$

This is more than three orders of magnitude greater than the maximum heat transfer rate needed to heat up the interior of the bubble, so we conclude that heat conduction across the thermal boundary layer presents no problem.

J. Vapor Entrainment Losses

The single most serious problem confronting the feasibility of the liquid core reactor is that of specific impulse degradation (and to a lesser extent, fuel inventory cost increase) due to contamination of the hydrogen exhaust gas with high-molecular mass fuel vapor (including the diluent as well as the fissionable material). It is clear

that fuel will tend to evaporate across the surface of each gas bubble in the core as well as across the inner surface of each fuel annulus in the core.

The first question which arises is whether or not a bubble achieves vapor pressure equilibrium by the time it completes its traversal of the fuel annulus. This matter is presently under detailed investigation. In the meantime, however, it is possible to predict the answer with some confidence, based on a simple physical consideration: The processes of heat conduction and mass diffusion obey the same mathematical relationship, viz., the classical Fourier heat conduction equation. It is not surprising, therefore, that both of these processes behave in the same way for any particular geometry. Since the boundary conditions for the heat conduction problem of Paragraph H are formally identical with those which apply to the question of whether or not vapor pressure equilibrium can be achieved in the interior of a bubble, we expect that the answer to the latter question will be closely related to the results of Paragraph H. In other words, if we arrange things (such as liquid/gas temperature gradients, fuel annulus thickness and bubble size) in such a way as to ensure that thermal equilibrium between a gas bubble and the liquid medium is reached by the time the bubble emerges from the fuel annulus, we may expect that vapor pressure equilibrium will also be reached.

Under the assumption that vapor pressure equilibrium exists, the analysis is quite simple. Recall that the fuel is a solution consisting of fissionable material (UC_2), the "solute", and diluent material (ZrC), the "solvent", in the ratio of d moles of the latter to each mole of the former. It is known that ZrC dissociates when it evaporates, i.e., it evaporates as Zr and C, never as ZrC. UC_2 probably behaves in a somewhat similar fashion, but since data are scant, let us make the slightly pessimistic assumption the UC_2 evaporates without any dissociation. Thus the mole fractions of UC_2 molecules and Zr and C atoms in the liquid phase are, respectively, $1/(d+1)$, $d/(d+1)$ and $d/(d+1)$. Since the solute and solvent are both carbides and therefore not grossly dissimilar substances, and since it is assumed that $d \gg 1$, we may expect that the fuel mixture is a reasonably good approximation to an ideal solution. By Henry's law,

$$p_{v_{UC_2}} = \frac{1}{d+1} \, p^{o}_{v_{UC_2}} , \qquad (290)$$

where $p_{v_{UC_2}}$ and $p^{o}_{v_{UC_2}}$ are the vapor pressures of the UC_2 solute in the fuel and of pure UC_2, respectively. Similarly, by Raoult's law,

$$p_{v_{Zr}} = \frac{d}{d+1} \, p^{o}_{v_{Zr}} , \qquad (291)$$

$$p_{v_C} = \frac{d}{d+1} p^{o}_{v_C} . \tag{292}$$

The mole fraction of each specie in the rocket exhaust is therefore

$$x_{UC_2} = \frac{1}{d+1} \frac{p^{o}_{v_{UC_2}}}{p_i} , \tag{293}$$

$$x_{Zr} = \frac{d}{d+1} \frac{p^{o}_{v_{Zr}}}{p_i} , \tag{294}$$

$$x_C = \frac{d}{d+1} \frac{p^{o}_{v_C}}{p_i} , \tag{295}$$

where p_i is the chamber pressure, i.e., the pressure in the central gas cavity of each fuel element.

Let $\dot{M}_H$, $\dot{M}_{UC_2}$, $\dot{M}_{Zr}$ and $\dot{M}_C$ be the mass flow rates of hydrogen, UC_2, Zr and C, respectively, for <u>all</u> the fuel elements. The sum of these is the total mass flow rate, $\dot{M}$. As a first approximation, let us assume that

$$\dot{M} = \dot{M}_H \tag{296}$$

and

$$\mathfrak{M} = \mathfrak{M}_H , \tag{297}$$

where $\mathfrak{M}_H$ is the mean molecular mass of an equilibrium composition of hydrogen just prior to expansion through the nozzle, and $\mathfrak{M}$ is the weighted average of the molecular masses of each specie. Then the molar flow rates of UC_2, Zr and C are, respectively,

$$\dot{n}_{UC_2} = x_{UC_2} \frac{\dot{M}_H}{\mathcal{M}_H} = \frac{1}{d+1} \frac{p^o_{v_{UC_2}}}{p_i} \frac{\dot{M}_H}{\mathcal{M}_H} , \tag{298}$$

$$\dot{n}_{Zr} = x_{Zr} \frac{\dot{M}_H}{\mathcal{M}_H} = \frac{d}{d+1} \frac{p^o_{v_{Zr}}}{p_i} \frac{\dot{M}_H}{\mathcal{M}_H} , \tag{299}$$

$$\dot{n}_C = x_C \frac{\dot{M}_H}{\mathcal{M}_H} = \frac{d}{d+1} \frac{p^o_{v_C}}{p_i} \frac{\dot{M}_H}{\mathcal{M}_H} . \tag{300}$$

The corresponding mass flow rates are therefore

$$\dot{M}_{UC_2} = \dot{n}_{UC_2} \mathcal{M}_{UC_2} = \frac{\dot{M}_H}{d+1} \frac{p^o_{v_{UC_2}}}{p_i} \frac{\mathcal{M}_{UC_2}}{\mathcal{M}_H} , \tag{301}$$

$$\dot{M}_{Zr} = \dot{n}_{Zr} \mathcal{M}_{Zr} = \frac{\dot{M}_H d}{d+1} \frac{p^o_{v_{Zr}}}{p_i} \frac{\mathcal{M}_{Zr}}{\mathcal{M}_H} , \tag{302}$$

$$\dot{M}_C = \dot{n}_C \mathcal{M}_C = \frac{\dot{M}_H d}{d+1} \frac{p^o_{v_C}}{p_i} \frac{\mathcal{M}_C}{\mathcal{M}_H} . \tag{303}$$

Of course, the mass flow rate of uranium is

$$\dot{M}_U = \frac{\mathcal{M}_U}{\mathcal{M}_{UC_2}} \dot{M}_{UC_2} . \tag{304}$$

The weighted average of the molecular masses is

$$\mathcal{M} = \frac{\dot{M}_H \mathcal{M}_H + \dot{M}_{UC_2} \mathcal{M}_{UC_2} + \dot{M}_{Zr} \mathcal{M}_{Zr} + \dot{M}_C \mathcal{M}_C}{\dot{M}} \tag{305}$$

where

$$\dot{M} = \dot{M}_H + \dot{M}_{UC_2} + \dot{M}_{Zr} + \dot{M}_C . \tag{306}$$

The computational procedure is as follows: Ideal (i.e., for an uncontaminated equilibrium composition of pure hydrogen) values for the vacuum specific impulse and molecular weight $\mathfrak{M}_H$ (before expansion) are obtained from Reference 4. Assuming a fixed thrust, F, we then find

$$\dot{M}_H = \frac{F}{I_{sp}} \quad . \tag{307}$$

$\dot{M}_{UC_2}$, $\dot{M}_{Zr}$, $\dot{M}_C$ and $\dot{M}$ are then found from Eqs. (301)-(303) and (306). The latter values are substituted into Eq. (305) to give $\mathfrak{M}$. The "corrected" specific impulse is then given by

$$I'_{sp} = \sqrt{\frac{\mathfrak{M}_H}{\mathfrak{M}}} \; I_{sp} \quad . \tag{308}$$

The next step is to calculate the corrected hydrogen mass flow rate, $\dot{M}'_H$, which is necessary in order that F be held constant:

$$\dot{M}'_H = \frac{F}{I'_{sp}} \quad . \tag{309}$$

The second approximations to $\dot{M}_{UC_2}$, $\dot{M}_{Zr}$ and $\dot{M}_C$, designated with primes, are:

$$\dot{M}'_{UC_2} = \frac{\dot{M}}{d+1} \; \frac{P^o_{v_{UC_2}}}{P_i} \; \frac{\mathfrak{M}_{UC_2}}{\mathfrak{M}} \quad , \tag{310}$$

$$\dot{M}'_{Zr} = \frac{\dot{M}_d}{d+1} \frac{P^o_{v_{Zr}}}{P_i} \frac{m_{Zr}}{m} , \tag{311}$$

$$\dot{M}'_{C} = \frac{\dot{M}_d}{d+1} \frac{P^o_{v_C}}{P_i} \frac{m_C}{m} . \tag{312}$$

Then

$$\dot{M}' = \dot{M}'_H + \dot{M}'_{UC_2} + \dot{M}'_{Zr} + \dot{M}'_C \tag{313}$$

and

$$m' = \frac{\dot{M}'_H m_H + \dot{M}'_{UC_2} m_{UC_2} + \dot{M}'_{Zr} m_{Zr} + \dot{M}'_C m_C}{\dot{M}'} . \tag{314}$$

Finally, we write

$$I''_{sp} = \sqrt{\frac{m'}{m}} \; I'_{sp} . \tag{315}$$

This process is repeated until

$$I^{(n)}_{sp} - I^{(n+1)}_{sp} \leq \epsilon , \tag{316}$$

where ϵ is some preselected maximum error, say 1 sec.

These calculations were performed on a digital computer, and results are plotted on various coordinates in Figures 14 through 18. The sample design point (P_c = 10 atm, d = 500 ZrC/UC_2) is shown as a small circle on each figure.

V. DISCUSSION OF RESULTS

Figures 13 through 17 indicate that although the maximum attainable specific impulse of the liquid-core

nuclear rocket appears to be lower than preliminary estimates indicated, performance levels are sufficiently high that further, more detailed studies are warranted. In particular, the present analysis demonstrates theoretical feasibility, subject, of course, to further evaluation of the validity of the assumptions on which the analysis is based.

The most significant features of the performance results (Figures 13-17) are the rather low pressures and temperatures required to maximize specific impulse. Note that the "feedback" of these optimizations, in particular that of the temperature*, has not yet been incorporated into the criticality estimate. Since the Maxwell-Boltzmann averaged cross section increases at lower temperatures this will have a small but finite effect in reducing reactor mass, or, alternatively, permitting an increase in the dilution ratio (ZrC/UC_2) to reduce the fractional loss of uranium carbide, and thereby achieve some improvement in specific impulse (since ZrC has a much lower vapor pressure then UC_2).

Another source for possible performance improvement may result from substitution of UC for UC_2, since there is some indication that the vapor pressure of the monocarbide may be lower than that of the dicarbide.

---

* See footnote on p. 5.

Unfortunately, unclassified vapor pressure data on UC are even more scant than results for UC_2, and therefore no quantitative basis for analysis of a monocarbide-fueled system could be established.

A third significant area for improvement is the substitution of U-233 for U-235 as the fissionable material. This was not considered initially because it was believed that system feasibility must first be demonstrated with U-235, with U-233 representing a possible growth potential. Nucleonic calculations using U-233 at the proper temperature level are now in process, and are expected to produce benefits of the same type as those resulting from the use of lower core temperatures.

A final possibility for improvement may be the partial replacement of U-235 (or U-233) by a nucleonically-equivalent (i.e.,larger) amount of thorium - 232, whose carbide has a vapor pressure about 20 times lower than that of UC_2. Unfortunately, Th-232 undergoes only fast fission and since the large amount of carbon in the core is quite effective as a moderator, it is conceivable that only small improvement, if any, may be realized.

In the area of operational characteristics, a conclusion of major importance, as analyzed in Section IV and shown in Figure 12, is that heat transfer does not limit either thrust level or performance. This conclusion

must, of course, be evaluated by high-gravity experimental studies which are now in the process of being formulated. Another potentially-limiting factor is the fuel-element rotational speed required to produce bubble velocities sufficiently high to provide adequate mass flow rate. For the selected engine thrust/weight ratios, speeds were quite reasonable; i.e., of the order of 5,000 rpm (see Figure 12). Since the overall pressure drop was also quite moderate, and the general core configuration at least approximates that of more conventional reactors, there do not appear to be any major inherent infeasibilities in the proposed concept. Subsequent studies of heat transfer and bubble flow characteristics at high gravities, "freezing-in" of gas passages on shutdown, significant material vapor-pressure behavior, and multi-group analyses of both criticality and nucleonic dynamics are planned to evaluate the various assumptions and approximations made in this preliminary study.

REFERENCES

1. Crocco, L., private communication.

2. Bussard, R. W., and DeLauer, R. D., "Nuclear Rocket Propulsion," McGraw-Hill, New York, 1958.

3. Glasstone, S., and Sesonske, A., "Nuclear Reactor Engineering," Van Nostrand, 1963.

4. King, C. R., "Compilation of Thermodynamic Properties, and Theoretical Rocket Performance of Gaseous Hydrogen," NASA Technical Note D-275, April, 1960.

5. Bussard, R. W., "Some Considerations of the Liquid Core Reactor Concept," unpublished memorandum dated March 23, 1961.

6. Shinnar, R., private communication.

7. Lamb, H., "Hydrodynamics," 6th ed., 1932, Dover reprint.

8. Chao, B. T., Physics of Fluids, 5, No. 1, p. 69, January, 1962.

9. Taylor, G. I., and Davies, R. M., "The Rate of Rise of Large Volumes of Gases in Water," Undex 88.

10. Carslaw, H. S., and Jaeger, J. C., "Conduction of Heat in Solids," 2nd ed., Oxford, 1959.

11. Nelson, S. T., unpublished memorandum.

12. "The Reactor Handbook," US AEC.

13. Janaf Thermochemcial Data, Dow Chemical Company.

TABLE I

PROPERTIES OF FUEL MATERIALS

	ZrC	UC_2
Molecular weight, (a.m.u.)	103.23	259.09
Density (gm/cm^3)	6.8	11.14
Melting Point (deg K)	3770	2530
Boiling Point, (deg K)	5370	4370

TABLE 2

PRELIMINARY RESULTS OF CRITICALITY ANALYSIS

	d	ν	f	k_∞	τ^* cm^2	L^{*2} (cm^2)	M^{*2} (cm^2)	$B_c^2 \times 10^3$ prelim (cm^{-2})
IA	5	.1	.998	2.056	432	10.18	442.18	2.390
IB	5	.2	.998	2.056	547	12.88	559.88	1.885
IC	5	.3	.998	2.056	714	16.83	730.83	1.445
ID	5	.4	.998	2.056	972	22.9	994.9	1.062
IE	5	.5	.998	2.050	1400	33.0	1433.0	0.737
IIA	10	.1	.996	2.050	432	20.35	452.35	2.325
IIB	10	.2	.996	2.050	547	25.8	572.80	1.835
IIC	10	.3	.996	2.050	714	33.65	747.65	1.405
IID	10	.4	.996	2.050	972	45.8	1017.8	1.032
IIE	10	.5	.996	2.050	1400	65.9	1465.9	0.717
IIIA	50	.1	.982	2.023	432	91.5	523.5	1.955
IIIB	50	.2	.982	2.023	547	115.9	662.9	1.543
IIIC	50	.3	.982	2.023	714	151.3	865.3	1.183
IIID	50	.4	.982	2.023	972	206.0	1178.0	0.868
IIIE	50	.5	.982	2.023	1400	296.5	1696.5	0.603
IVA	100	.1	.965	1.990	432	178.2	610.2	1.623
IVB	100	.2	.965	1.990	547	225.5	772.5	1.282
IVC	100	.3	.965	1.990	714	294.5	1008.5	0.982
IVD	100	.4	.965	1.990	972	424.5	1396.5	0.710
IVE	100	.5	.965	1.990	1400	577.5	1977.5	0.501
VA	500	.1	.846	1.743	432	275.	707.	1.053
VB	500	.2	.846	1.743	547	348.	895.	0.831
VC	500	.3	.846	1.743	714	455.	1169.	0.637
VD	500	.4	.846	1.743	972	620.	1592.	0.467
VE	500	.5	.846	1.743	1400	892.	2292.	0.3245
VIA	1000	.1	.733	1.510	432	1360.	1792.	0.2845
VIB	1000	.2	.733	1.510	547	1720.	2267.	0.2250
VIC	1000	.3	.733	1.510	714	2245.	2959.	0.1725
VID	1000	.4	.733	1.510	972	3060.	4032.	0.1265
VIE	1000	.5	.733	1.510	1400	4400.	5800.	0.8800

TABLE 3

RESULTS OF REACTOR ANALYSIS

CASE	d	$\sqrt{}$	[cm] R_c	[cm] R	[cm] D_t	[ft] D_t	[cm] L	[m^3] V	[m^3] V_f	metric tons M_f	metric tons M_{UC_2}	metric tons M_U	mega-bucks U-cost	metric tons M_{refl}	metric tons M_t	ρ_f [gm/cm^3]
IA	5	.1	64.8	48.8	139.6	4.58	146.4	1.09	0.98	9.80	3.34	3.03	30.35	3.33	13.13	9.96
IB	5	.2	73.0	57.0	156.0	5.12	219.0	1.74	1.39	13.88	4.74	4.30	43.00	4.28	18.16	9.96
IC	5	.3	83.6	67.6	177.2	5.82	202.8	2.90	2.03	20.25	6.92	6.28	62.80	5.75	26.00	9.96
ID	5	.4	97.5	81.5	205.0	6.73	244.5	5.09	3.05	30.43	10.38	9.42	94.25	8.01	38.44	9.96
IE	5	.5	116.9	100.9	243.8	8.00	302.7	9.68	4.84	48.20	16.45	14.92	14.92	11.81	60.01	9.96
IIA	10	.1	65.8	49.8	141.6	4.65	149.4	1.16	1.04	8.89	1.78	1.61	16.15	3.40	12.29	8.49
IIB	10	.2	74.1	58.1	158.2	5.19	174.3	1.84	1.47	12.53	2.51	2.27	22.79	4.42	16.95	8.49
IIC	10	.3	84.5	68.5	179.0	5.83	205.5	3.02	2.11	17.97	3.60	3.26	32.67	5.89	23.86	8.49
IID	10	.4	98.8	82.8	207.6	6.80	248.4	5.34	3.20	27.21	5.45	4.94	49.40	8.24	35.45	8.49
IIE	10	.5	118.3	102.3	246.6	8.10	337.5	10.08	5.04	42.80	9.57	8.68	86.85	12.13	54.93	8.49
IIIA	50	.1	71.2	55.2	152.4	5.00	165.6	1.58	1.42	10.17	0.48	0.44	4.40	4.05	14.22	7.13
IIIB	50	.2	80.2	64.2	170.4	5.60	192.6	2.49	1.99	14.21	0.67	0.61	6.15	5.26	19.47	7.13
IIIC	50	.3	91.5	75.5	193.0	6.33	226.5	4.05	2.83	20.22	0.96	0.87	8.76	6.99	27.21	7.13
IIID	50	.4	106.7	90.7	223.4	7.33	272.1	7.02	4.21	30.06	1.43	1.30	13.00	9.70	39.76	7.13
IIIE	50	.5	128.0	112.0	266.0	8.73	336.0	13.22	6.61	47.20	2.24	2.04	20.40	14.29	61.49	7.13
IVA	100	.1	77.0	61.0	164.0	5.38	183.0	2.13	1.92	13.39	0.32	0.29	2.97	4.81	18.20	6.96
IVB	100	.2	86.8	70.8	183.6	6.03	212.4	3.34	2.67	18.59	0.45	0.41	4.12	6.23	24.82	6.96
IVC	100	.3	99.0	83.0	208.0	8.83	249.0	5.37	3.76	26.20	0.64	0.58	5.81	8.28	34.48	6.96
IVD	100	.4	116.3	100.3	242.6	7.97	300.9	9.50	5.70	39.65	0.96	0.87	8.79	11.67	51.32	6.96
IVE	100	.5	138.8	122.8	287.6	9.94	368.4	17.44	8.72	60.67	1.48	1.34	13.45	16.90	77.57	6.96
VA	500	.1	91.8	75.8	193.6	6.35	227.4	4.10	3.69	25.20	0.125	0.113	1.13	7.04	32.24	6.83
VB	500	.2	103.2	87.2	216.4	7.12	261.6	6.24	4.99	34.15	0.167	0.151	1.51	9.05	43.20	6.83
VC	500	.3	117.8	101.8	245.6	8.06	305.4	9.95	6.96	47.60	0.236	0.215	2.15	12.00	59.60	6.83
VD	500	.4	137.5	121.5	285.0	9.35	364.5	16.88	10.12	69.25	0.344	0.312	3.12	16.62	85.87	6.83
VE	500	.5	163.9	147.9	337.8	11.08	436.7	30.45	15.22	104.0	0.518	0.471	4.71	24.0	128.0	6.83
VIA	1000	.1	163.7	147.7	337.4	11.07	443.1	30.30	27.27	186.1	0.464	0.422	4.22	23.9	210.0	6.80
VIB	1000	.2	183.7	167.7	377.4	12.40	503.1	44.35	35.48	241.4	0.604	0.548	5.48	30.4	271.8	6.80
VIC	1000	.3	210.0	194.0	430.0	14.1	582.0	68.75	48.12	327.0	0.817	0.742	7.42	40.1	367.1	6.80
VID	1000	.4	244.7	228.7	499.4	16.4	686.1	112.7	67.62	460.0	1.150	1.044	10.44	55.0	515.0	6.80
VIE	1000	.5	293.6	477.6	597.2	19.6	832.8	201.5	100.75	686.0	1.715	1.555	15.55	80.0	766.0	6.80

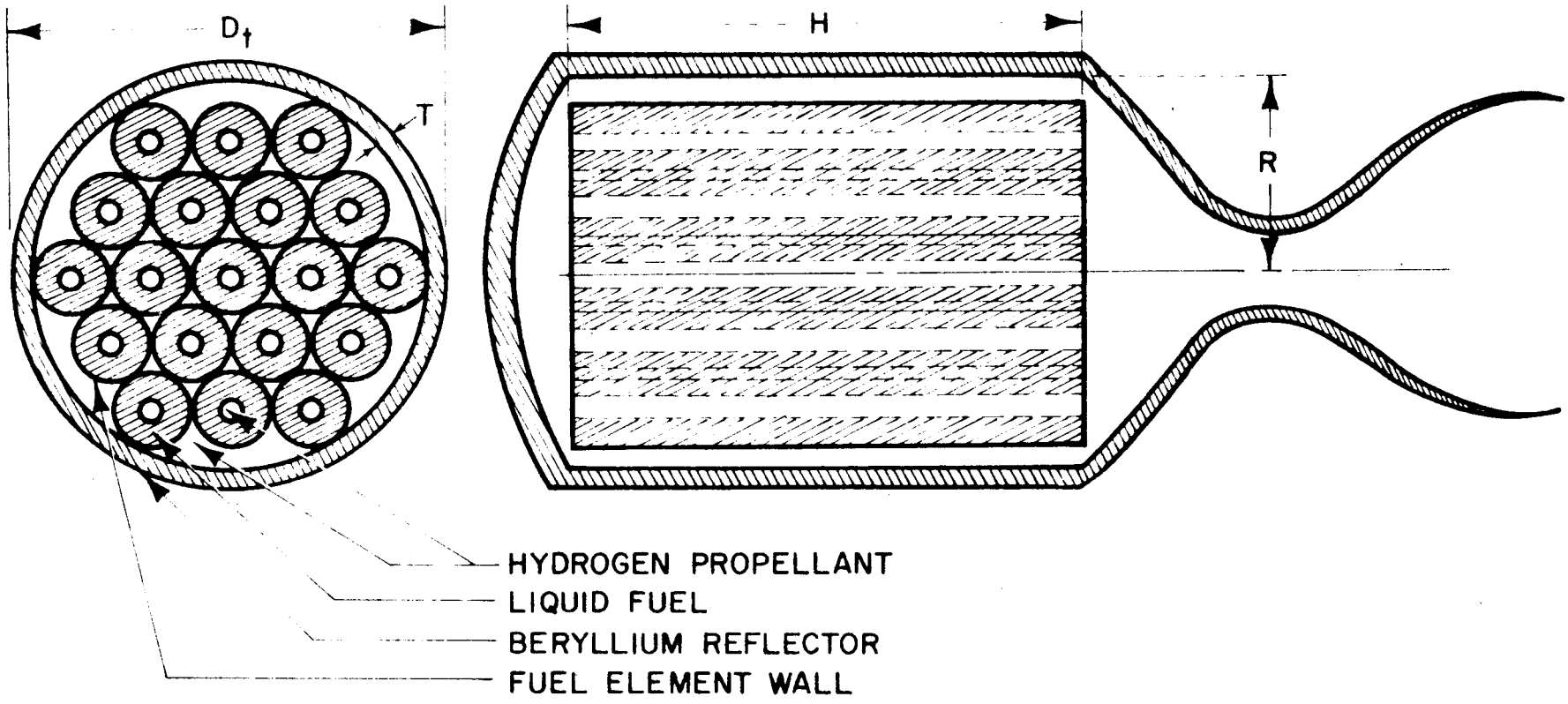

FIGURE 1

GEOMETRY OF THE LIQUID CORE REACTOR
(MATRIX SHOWN: N=19, P=5)

JPR2094

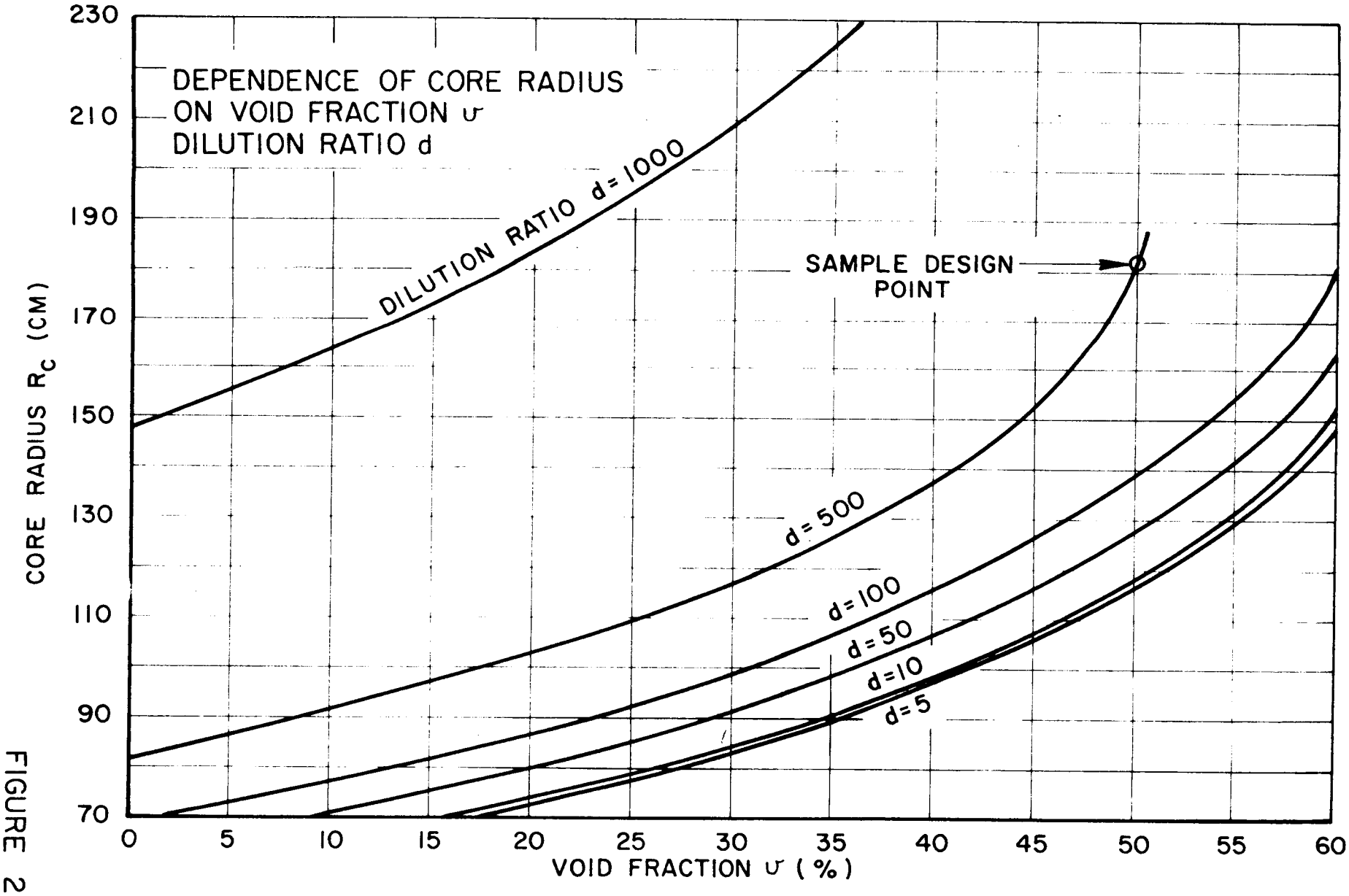

FIGURE 2

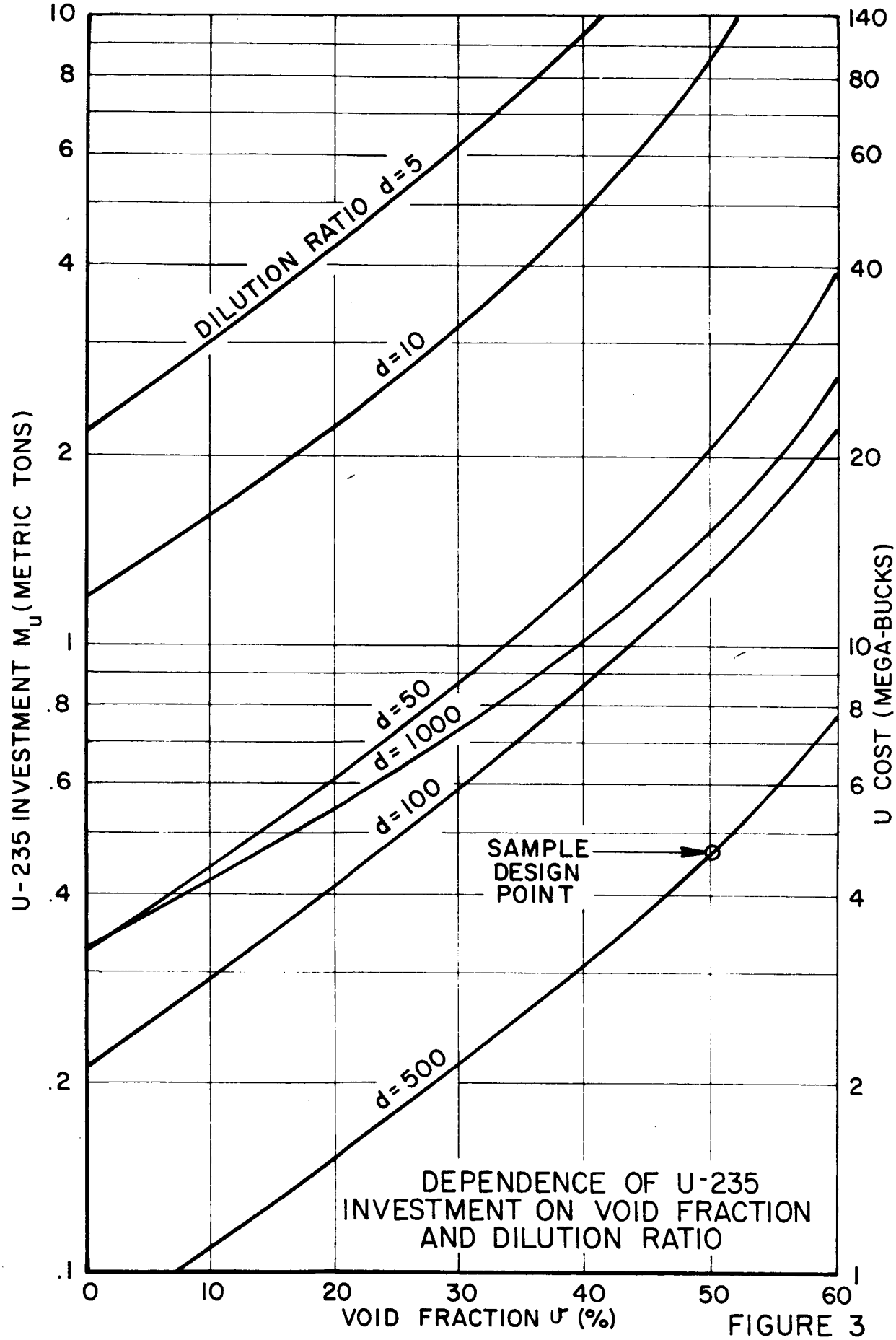

DEPENDENCE OF U-235 INVESTMENT ON VOID FRACTION AND DILUTION RATIO

FIGURE 3

JPR 2102

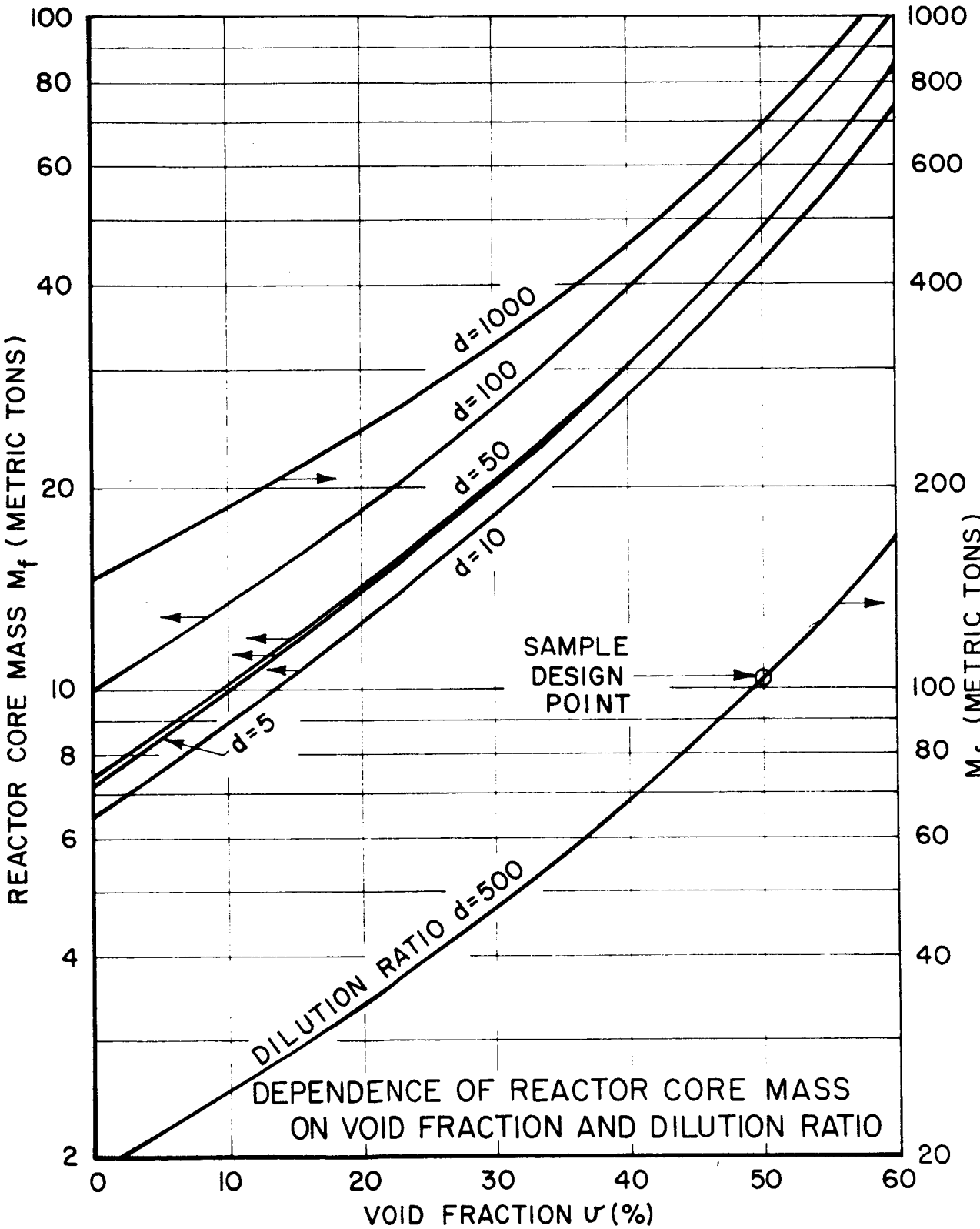

JPR2103

FIGURE 4

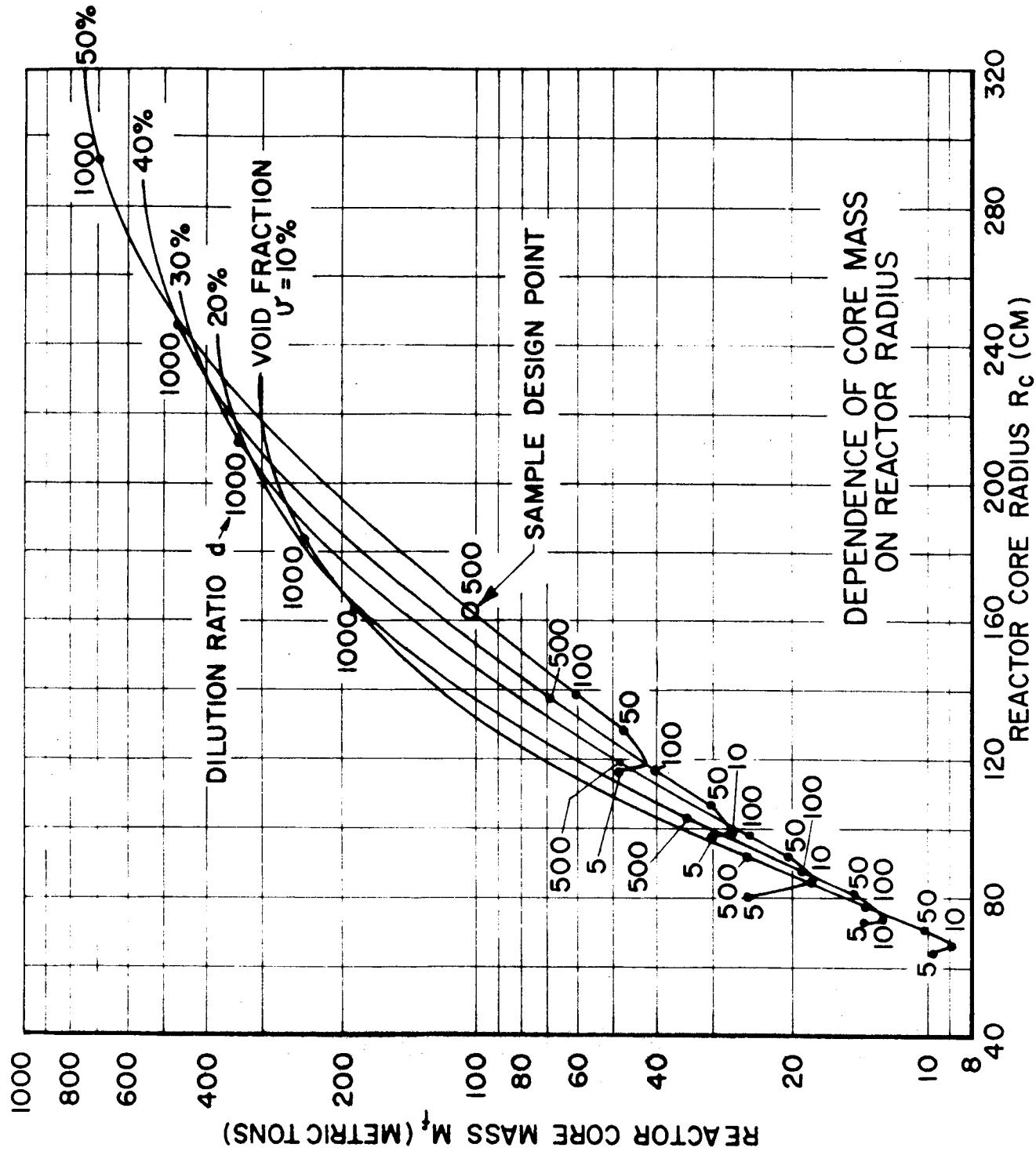

FIGURE 5

JPR2097

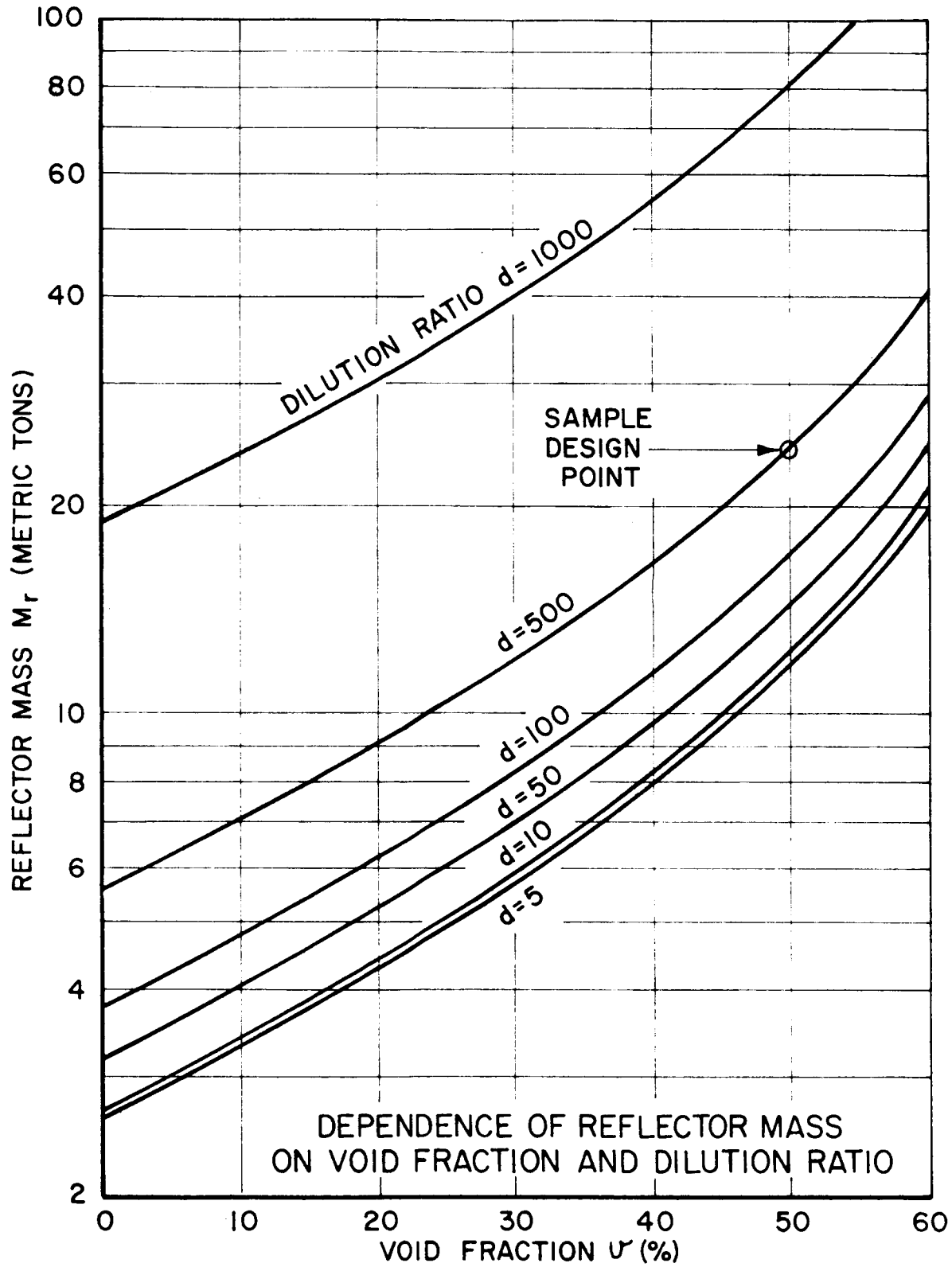

JPR2107

FIGURE 6

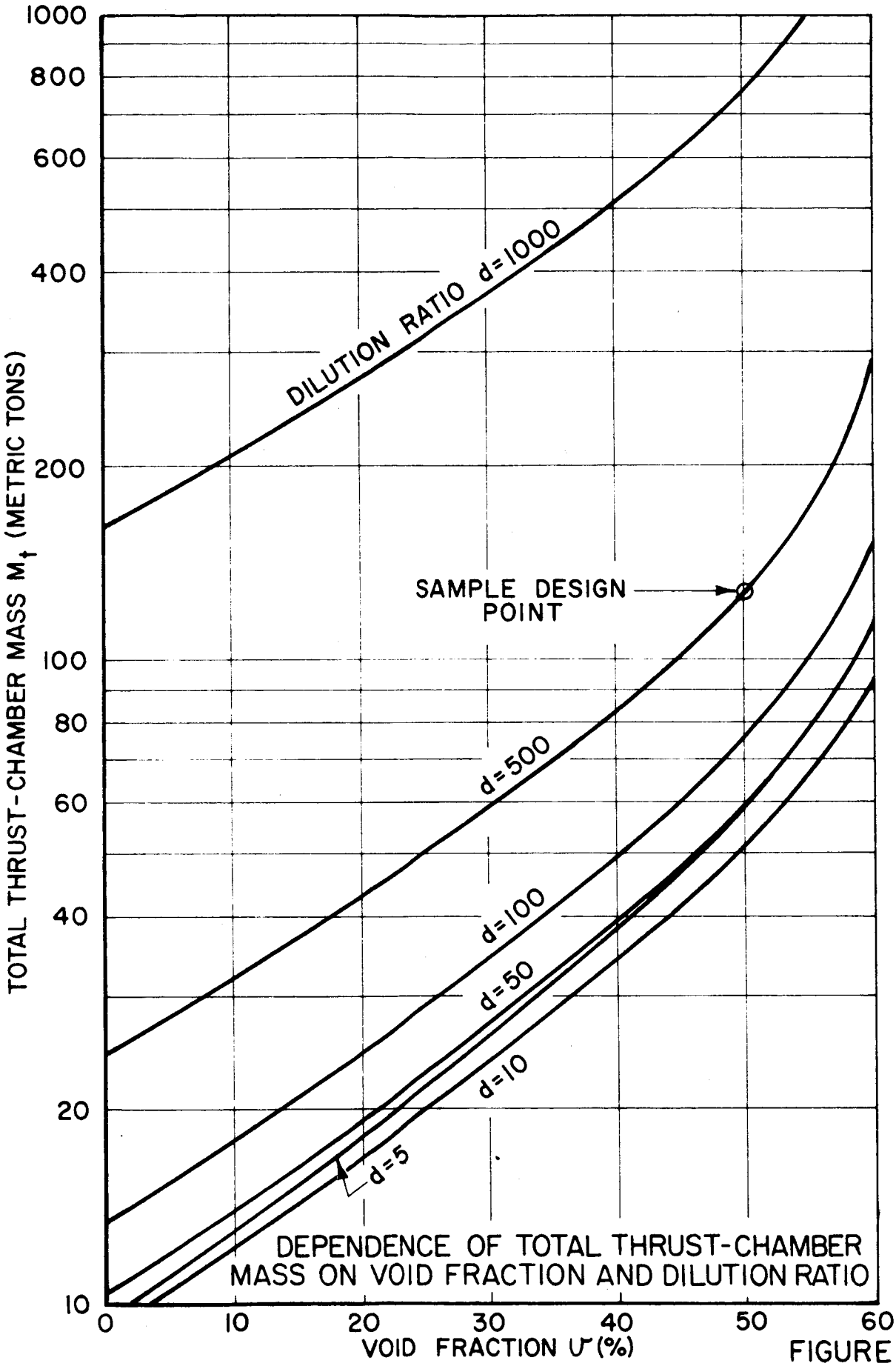

DEPENDENCE OF TOTAL THRUST-CHAMBER MASS ON VOID FRACTION AND DILUTION RATIO

FIGURE 7

JPR 2105

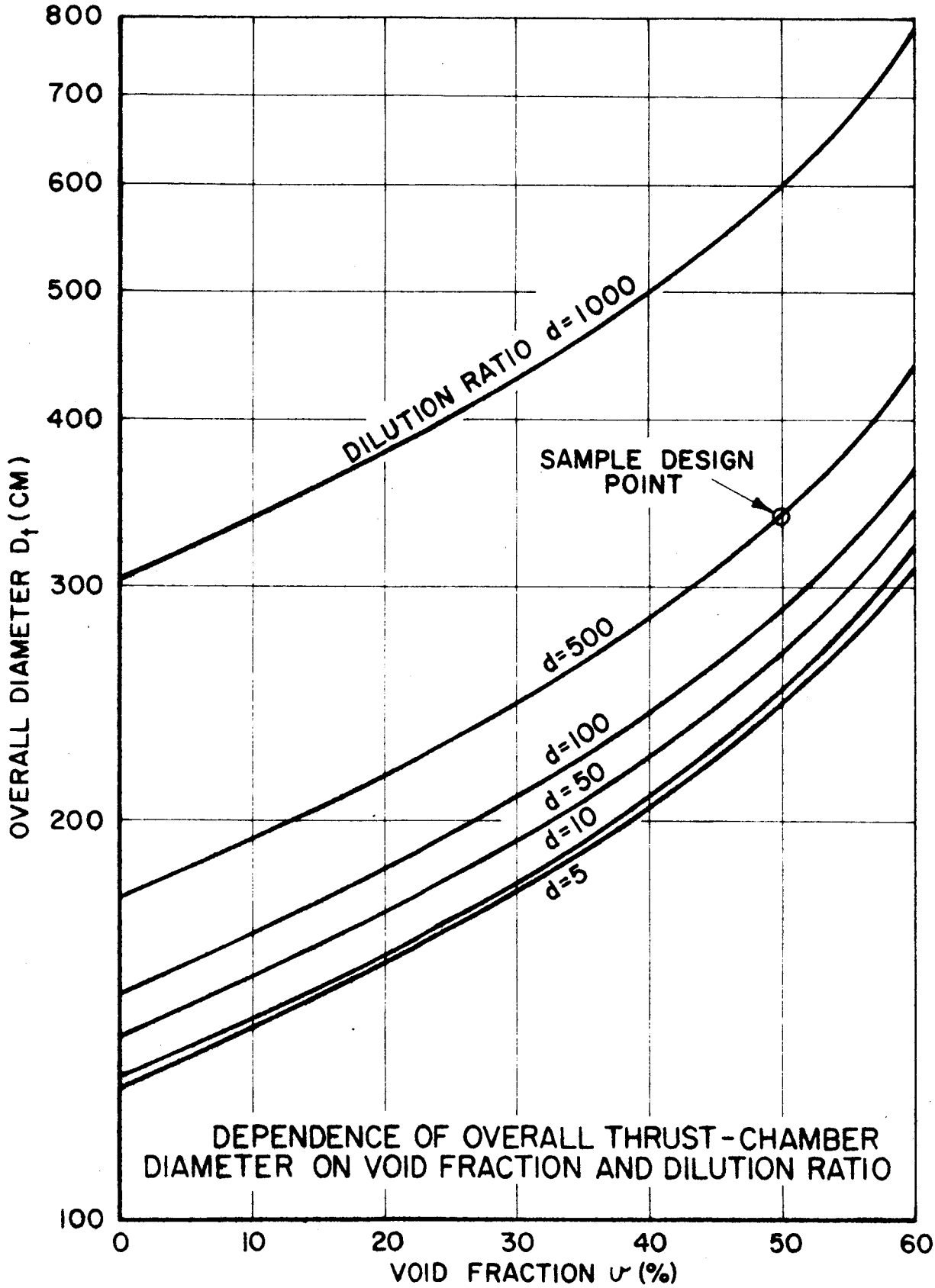

DEPENDENCE OF OVERALL THRUST-CHAMBER DIAMETER ON VOID FRACTION AND DILUTION RATIO

FIGURE 8

JPR2108

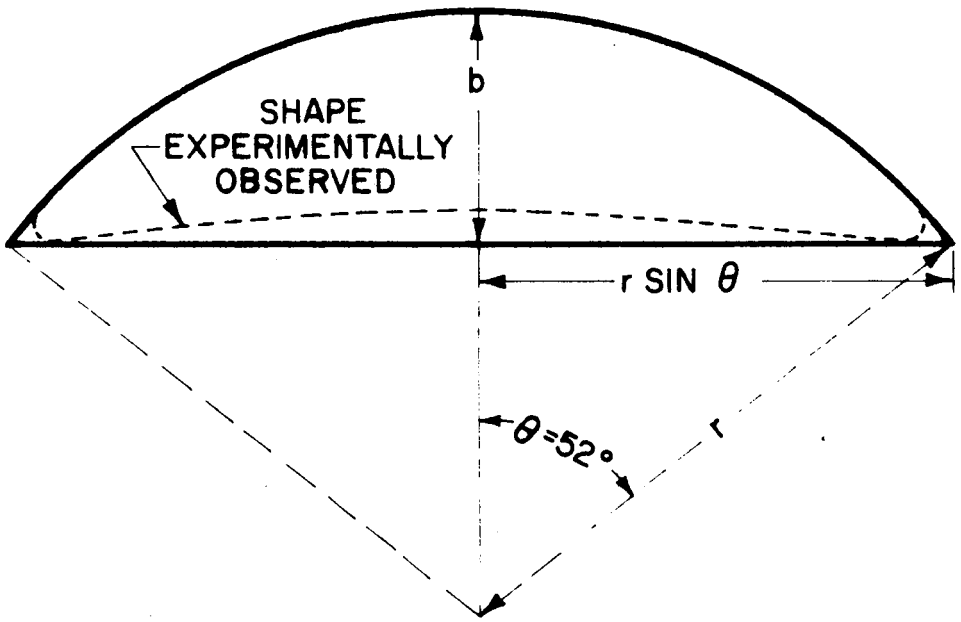

GEOMETRY OF THE SPHERICAL CAP BUBBLE

FIGURE 9

JPR2098

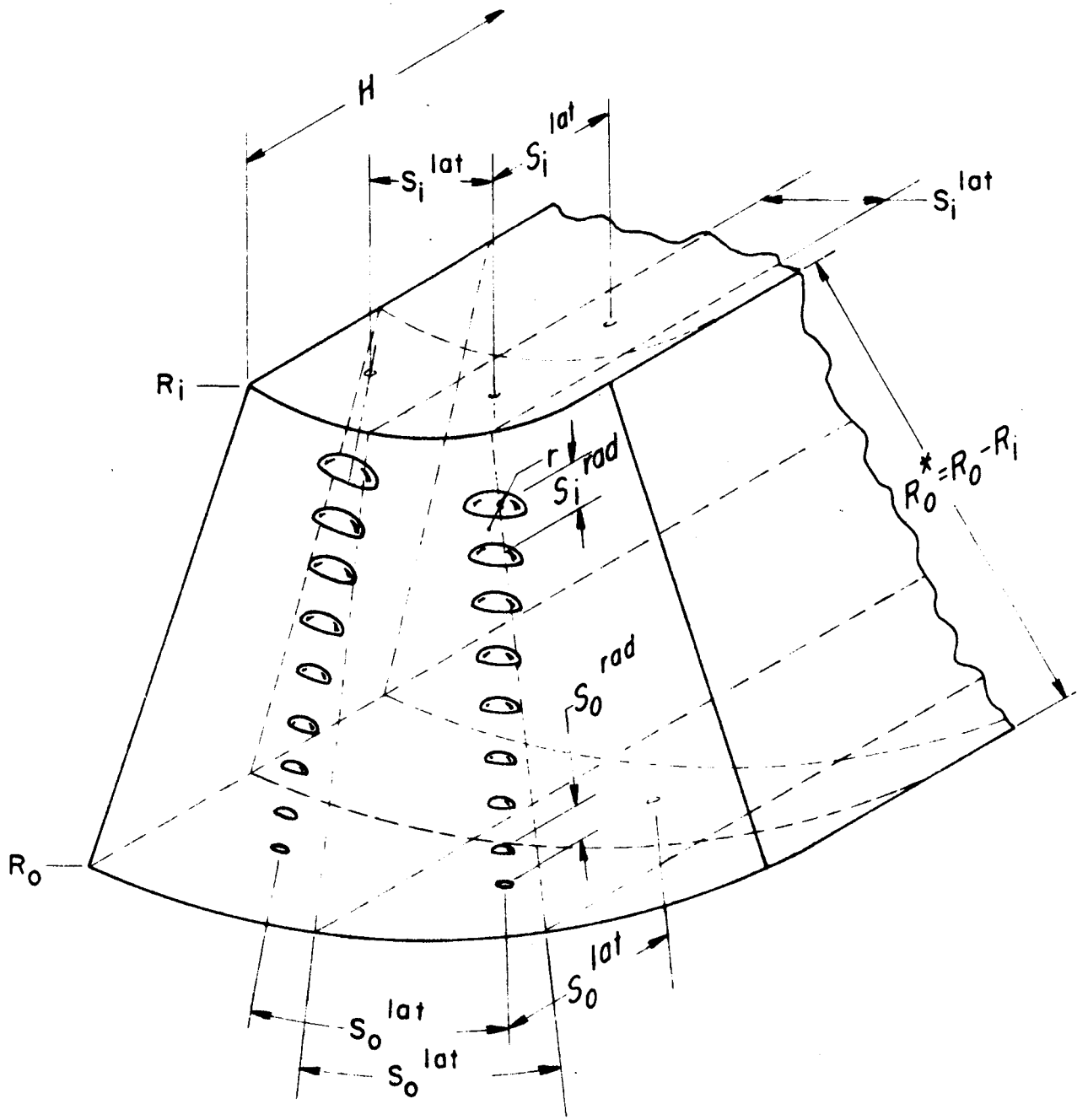

BUBBLE DISTRIBUTION WITHIN FUEL ELEMENT

JPR2101

FIGURE 10

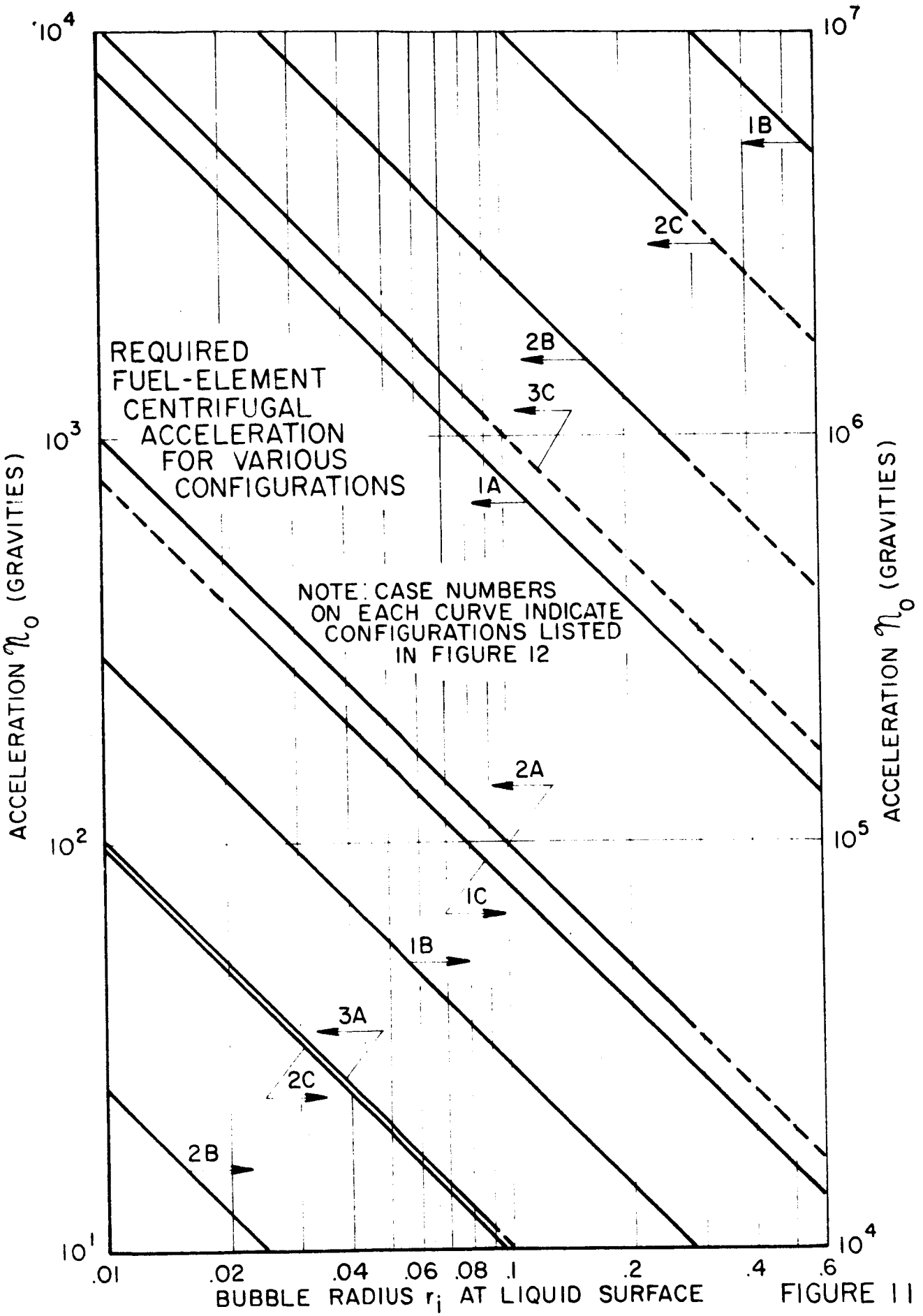

FIGURE 11

JPR2109

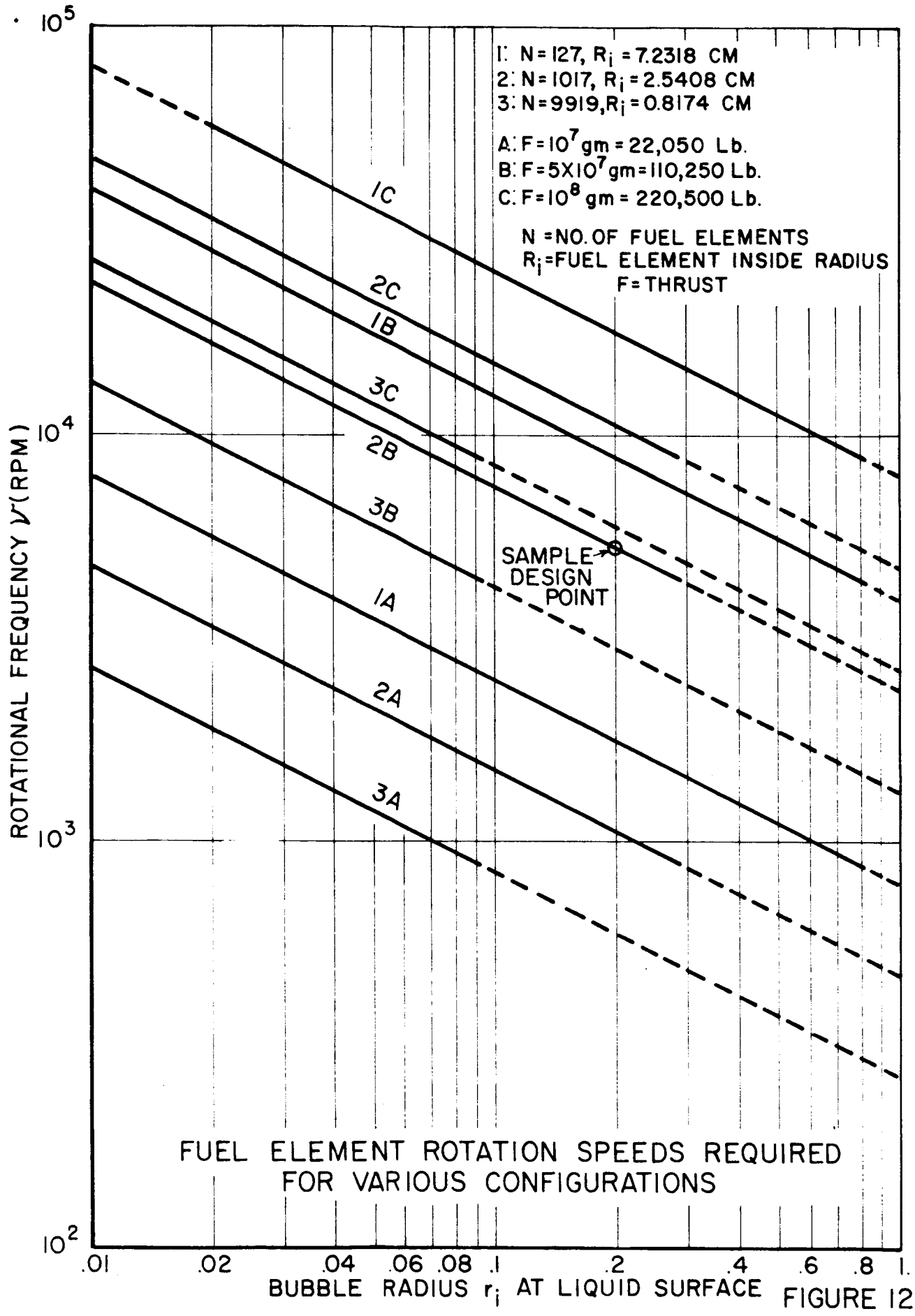

FUEL ELEMENT ROTATION SPEEDS REQUIRED FOR VARIOUS CONFIGURATIONS

FIGURE 12

JPR 2092

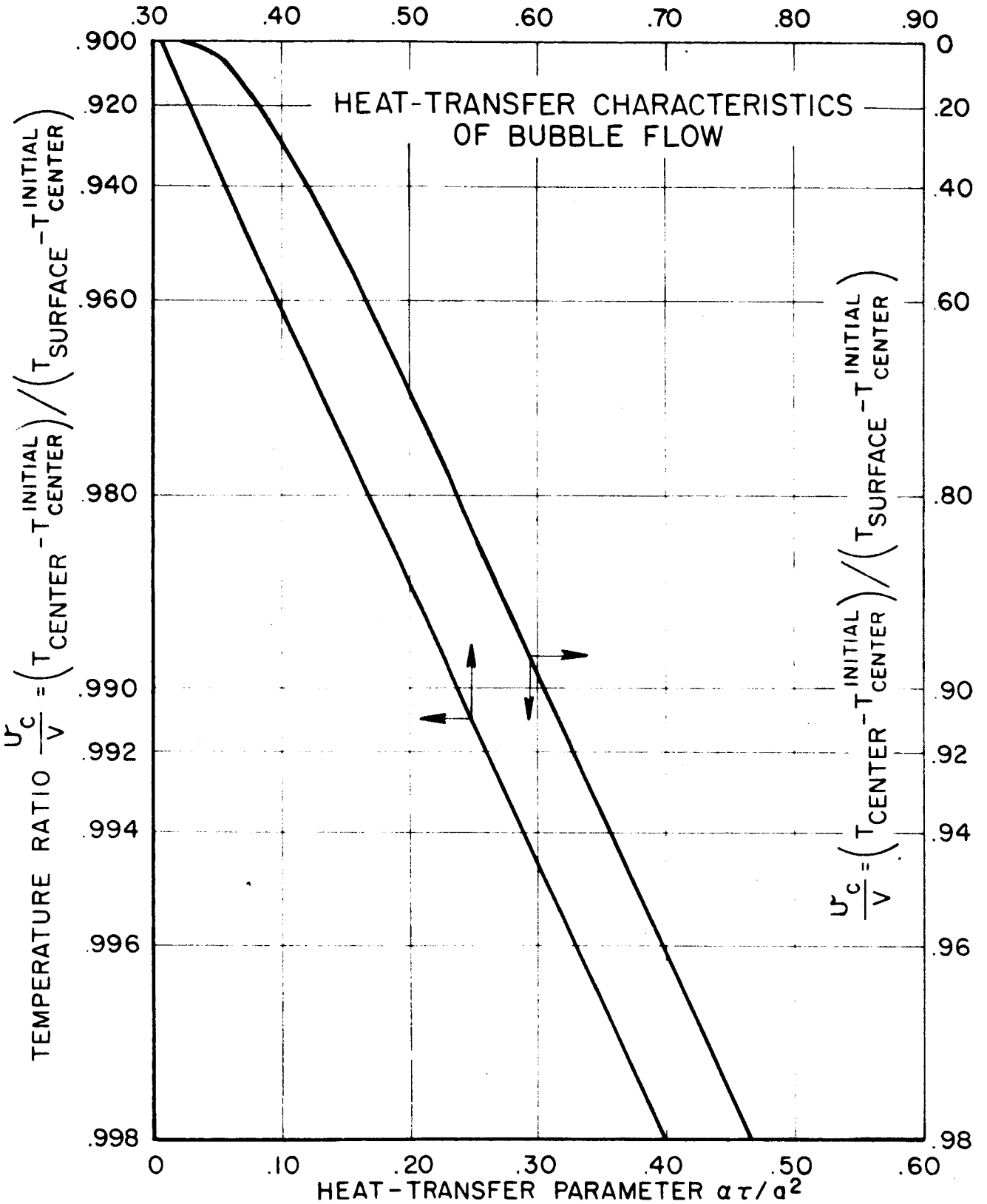

JPR 2104

FIGURE 13

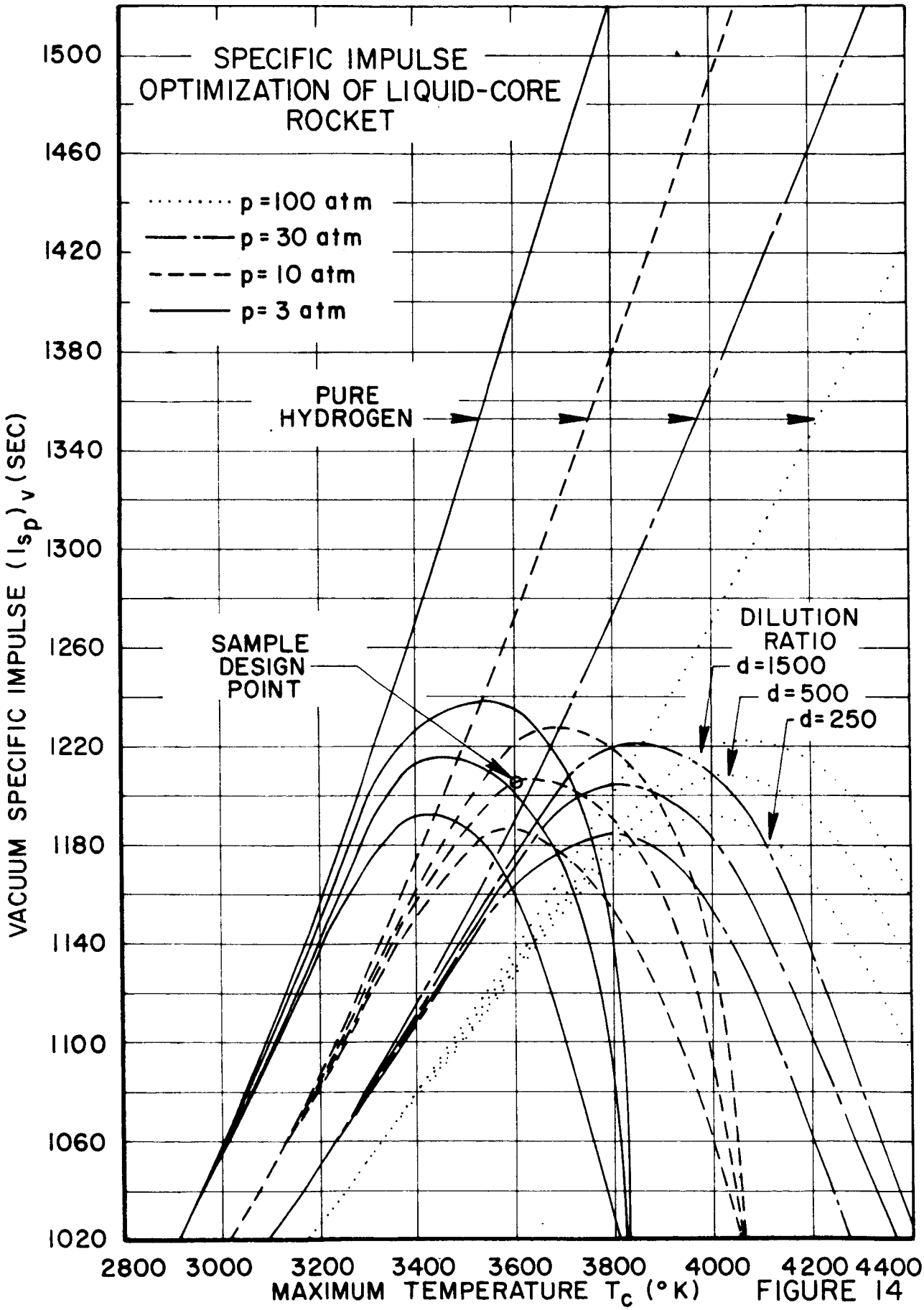

FIGURE 14

JPR 2099

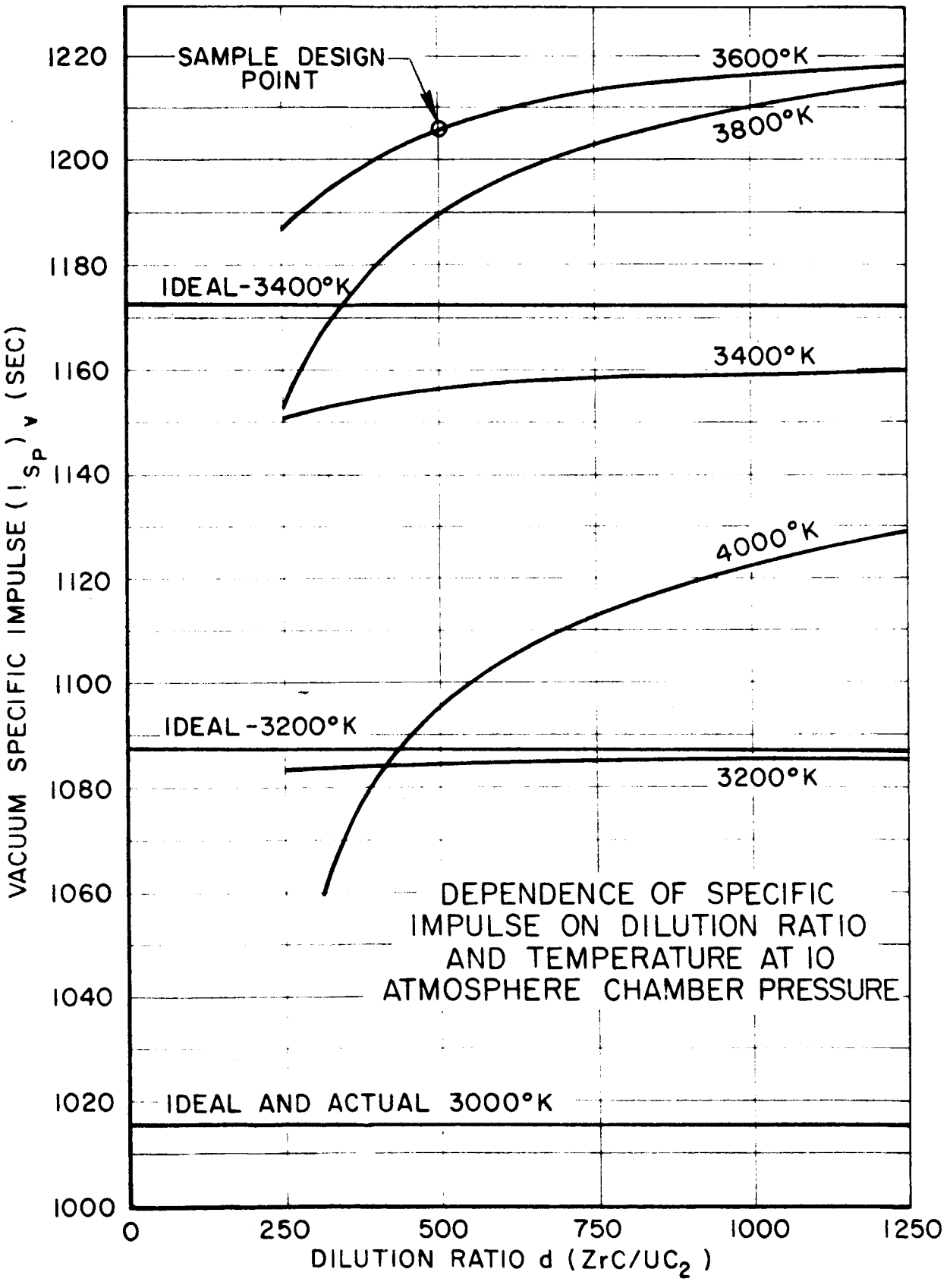

FIGURE 15

JPR2100

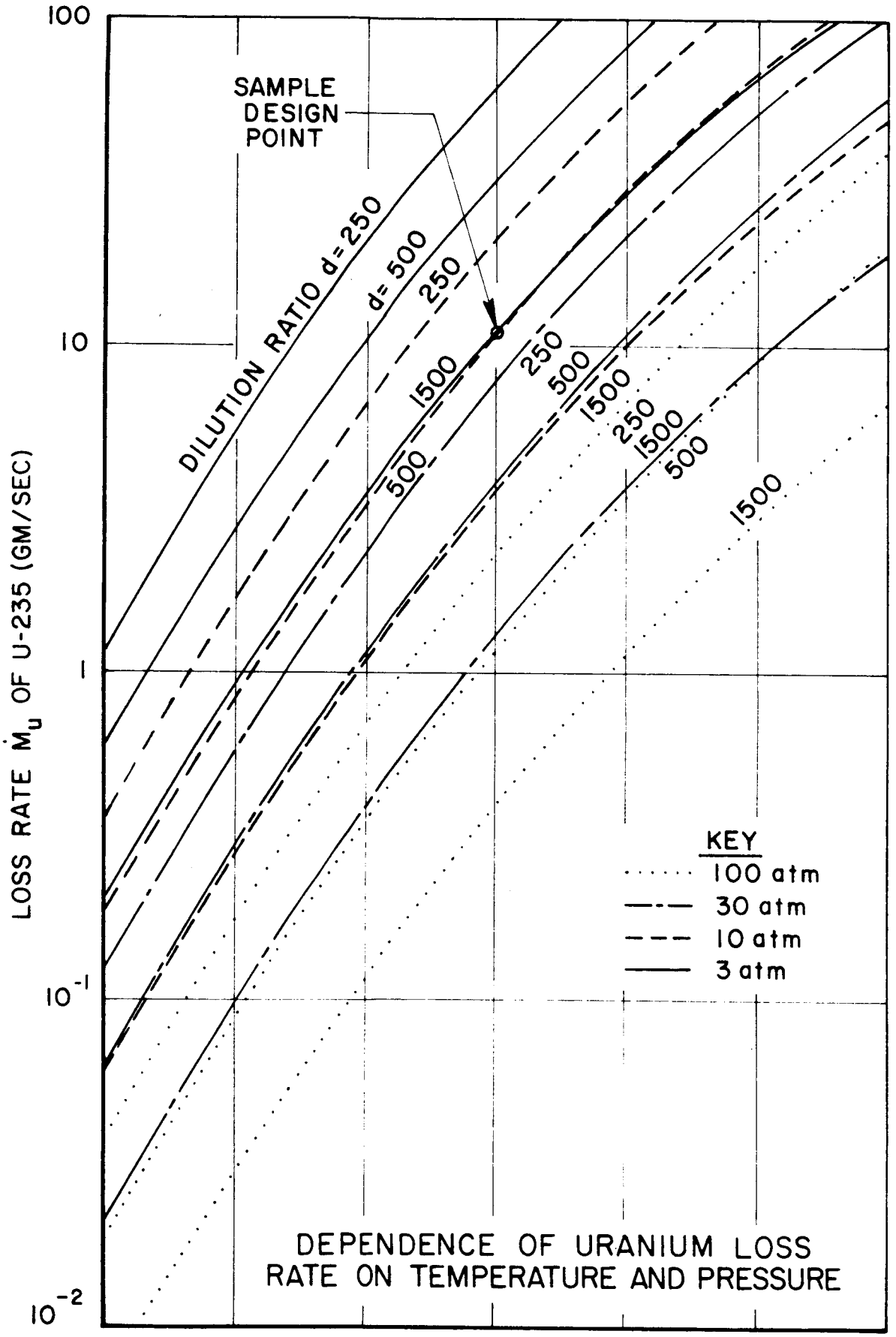

DEPENDENCE OF URANIUM LOSS RATE ON TEMPERATURE AND PRESSURE

FIGURE 16

JPR2095

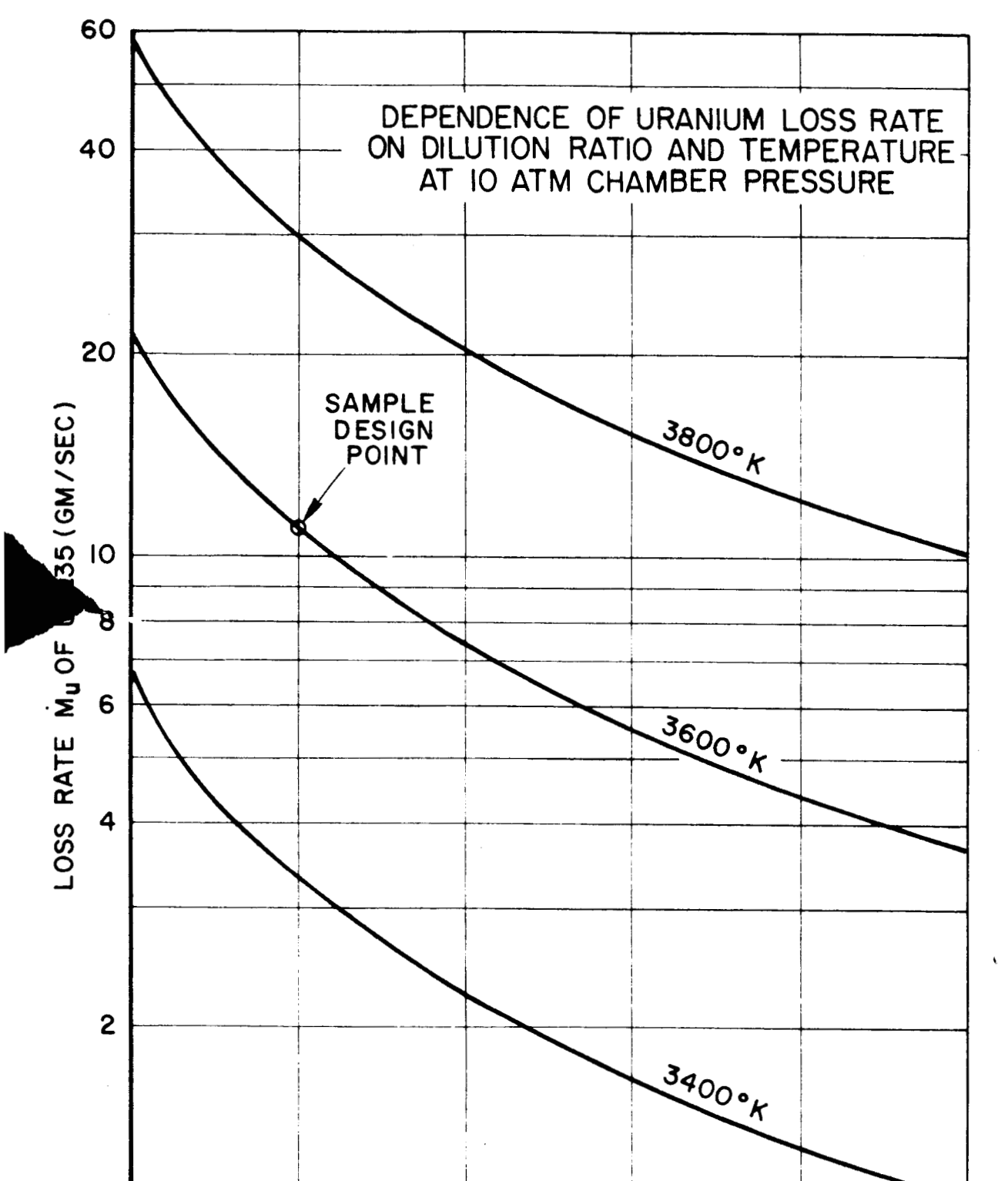
DEPENDENCE OF URANIUM LOSS RATE
ON DILUTION RATIO AND TEMPERATURE
AT 10 ATM CHAMBER PRESSURE
SAMPLE
DESIGN
POINT
3800°K
3600°K
3400°K
LOSS RATE $\dot{M}_u$ OF U-235 (GM/SEC)
60
40
20
10
8
6
4
2
1
250
500
750
1000
1250
1500
DILUTION RATIO d (ZrC/UC_2)

FIGURE 17

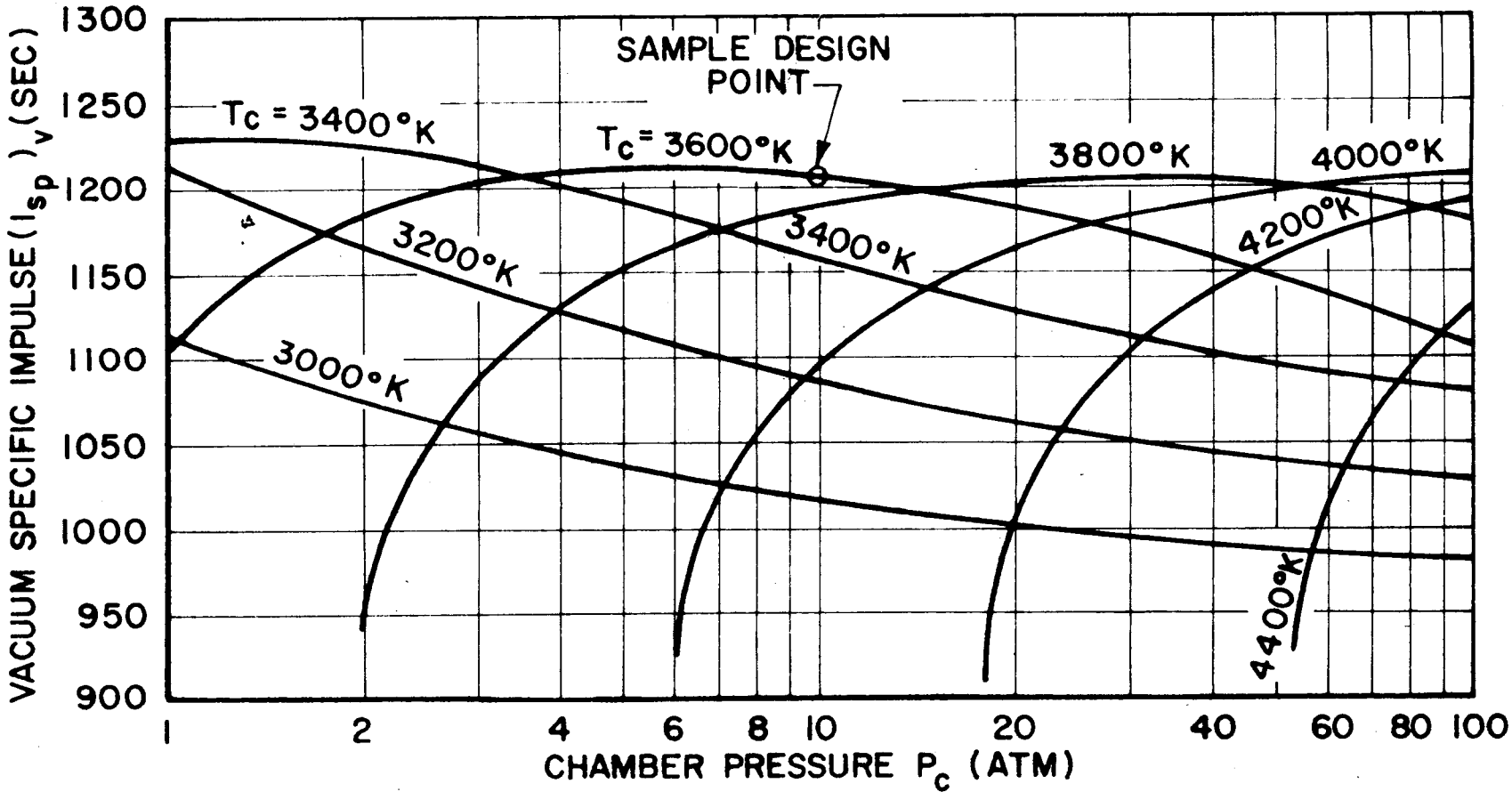

DEPENDENCE OF SPECIFIC IMPULSE ON CHAMBER PRESSURE AND TEMPERATURE (EXPANSION RATIO=500)

FIGURE 18